# The paleoclimate context and future trajectory of extreme summer hydroclimate in eastern Australia

Benjamin I Cook[1,2], Jonathan G Palmer[3], Edward R Cook[2], Chris S M Turney[3], Kathryn Allen[4], Pavla Fenwick[5], Alison O'Donnell[6], Janice M Lough[7], Pauline F Grierson[6], Michelle Ho[8], and Patrick J Baker[9]

[1]NASA Goddard Institute for Space Studies, New York, New York, USA

[2]Lamont-Doherty Earth Observatory, Palisades, New York, USA

[3]Climate Change Research Centre, School of Biological, Earth and Environmental Sciences, University of New South Wales, Sydney, New South Wales, Australia

[4]Department of Ecosystem and Forest Science, Melbourne School of Land and Environment, University of Melbourne, Richmond, Victoria, Australia

[5]Gondwana Tree-ring Laboratory, Little River, Canterbury, New Zealand

[6]Ecosystems Research Group, School of Plant Biology, The University of Western Australia, Crawley, Western Australia, Australia

[7]Australian Institute of Marine Science, Townsville, Queensland, Australia

[8]Columbia Water Center, Columbia University, New York City, New York, USA

[9]School of Ecosystem and Forest Sciences, University of Melbourne, Richmond, Victoria, Australia

**Main point #1**: Recent extremes (the Millennium Drought and 2011 pluvial) are compared to a 500-year soil moisture reconstruction

**Main point #2**: 2011 was likely the wettest year in the record for Coastal Queensland

**Main point #3**: Climate projections indicate substantially increased risk of droughts $\geq$ the magnitude of the Millennium Drought

Corresponding author: Benjamin I Cook, NASA Goddard Institute for Space Studies, New York, New York, USA. (benjamin.i.cook@nasa.gov)

**Abstract.** Eastern Australia recently experienced an intense drought (Millennium Drought, 2003–2009) and record-breaking rainfall and flooding (austral summer 2010–2011). There is some limited evidence for a climate change contribution to these events, but such analyses are hampered by the paucity of information on long-term natural variability. Analyzing a new reconstruction of summer (December–January–February) Palmer Drought Severity Index (the Australia–New Zealand Drought Atlas; ANZDA, 1500–2012 CE), we find moisture deficits during the Millennium Drought fall within the range of the last 500 years of natural hydroclimate variability. This variability includes periods of multi-decadal drought in the 1500s more persistent than any event in the historical record. However, the severity of the Millennium Drought, which was caused by autumn (March–April–May) precipitation declines, may be underestimated in the ANZDA because the reconstruction is biased towards summer and antecedent spring (September-October-November) precipitation. The pluvial in 2011, however, which was characterized by extreme summer rainfall faithfully captured by the ANZDA, is likely the wettest year in the reconstruction for Coastal Queensland. Climate projections (RCP 8.5 scenario) suggest that eastern Australia will experience long-term drying during the 21$^{st}$ century. While the contribution of anthropogenic forcing to recent extremes remains an open question, these projections indicate an amplified risk of multi-year drought anomalies matching or exceeding the intensity of the Millennium Drought.

## 1. Introduction

At the turn of the 21st century, two extreme hydroclimate events occurred over eastern Australia in rapid succession. The first was an intense, multi-year drought referred to as the Big Dry or Millennium Drought [*Cai et al.*, 2014; *Ummenhofer et al.*, 2009; *Verdon-Kidd and Kiem*, 2009]. From the late 1990s through 2009, precipitation deficits (primarily during austral autumn) contributed to low runoff and streamflow in the Murray-Darling Basin [*Kiem and Verdon-Kidd*, 2010; *Kirby et al.*, 2014; *Potter et al.*, 2010], caused fires across southeastern Australia [*Cai et al.*, 2009a; *Heberger*, 2011] including the Black Saturday fires that claimed 173 lives and cost an estimated US$3 billion [*Cai et al.*, 2009a; *Teague et al.*, 2010], and led to major economic and agricultural losses [*van Dijk et al.*, 2013; *Horridge et al.*, 2005; *Kirby et al.*, 2014]. Two years after the Millennium Drought, eastern Australia went on to experience one of the wettest summers on record [*Post et al.*, 2014; *Cai and van Rensch*, 2012], including record high rainfall in December of 2010 [*Australian Bureau of Meteorology*, 2011] and flooding in southeast Queensland and Brisbane in January 2011 that claimed 23 lives and caused US$2.55 billion in damages [*van den Honert and McAneney*, 2011]. The global land precipitation anomaly that year, associated with a major La Niña event, was so large that it caused a transient drop in global sea levels [*Boening et al.*, 2012; *Fasullo et al.*, 2013] and a record high terrestrial carbon sink [*Le Quéré et al.*, 2013; *Poulter et al.*, 2014].

Extreme droughts and floods are recurring features of the climate in eastern Australia, and the historical record is replete with examples. These include the Federation (1895–1902) and World War II (1937–1945) droughts [*Ummenhofer et al.*, 2009; *Verdon-Kidd*

*and Kiem*, 2009], the 1791–1792 Settlement Drought following initial European colonization [*Palmer et al.*, 2015; *Russell*, 1877], and numerous major floods [*van den Honert and McAneney*, 2011; *Pittock et al.*, 2006]. Hydroclimate in southern and eastern Australia is closely connected to three primary patterns of ocean-atmosphere variability that operate on interannual to multi-decadal timescales: the El Niño Southern Oscillation [ENSO; *Cai et al.*, 2011; *Nicholls et al.*, 1996; *Power et al.*, 1998], the Indian Ocean Dipole [IOD; *Cai et al.*, 2011; *Ummenhofer et al.*, 2009, 2011], and the Interdecadal Pacific Oscillation [IPO; *Kiem and Franks*, 2004; *Vance et al.*, 2015]. Precipitation over eastern Australia is generally suppressed during warm or positive phases of these modes, with each mode exhibiting strong seasonal biases in their teleconnections over eastern Australia. ENSO has the strongest and most widespread impact in spring (September-October-November; SON) and some modest strength during winter (June-July-August; JJA) [*Risbey et al.*, 2009]. Significant summer-season (December-January-February; DJF) ENSO teleconnections are localized primarily over Queensland and are weak and mostly non-significant during the autumn (March-April-May; MAM). The influence of the IOD is strongest from winter through the early spring (June–October), and is strongly amplified when a positive (negative) IOD event coincides with an El Niño (La Niña) [*Risbey et al.*, 2009]. The IPO primarily modulates the expression of ENSO variability, especially over Queensland [*Cai et al.*, 2010; *Cai and van Rensch*, 2012; *Kiem et al.*, 2003; *Kiem and Franks*, 2004; *Power et al.*, 1999], and appears to be most strongly connected with summer precipitation and drought [*Palmer et al.*, 2015; *Vance et al.*, 2015].

Precipitation deficits during the Millennium and other historical (Federation and World War II) droughts have been attributed to a range of phenomena. Some have pointed

to a consistent absence of rainfall-enhancing negative IOD events [*Ummenhofer et al.*, 2009, 2011]. Other analyses have suggested a more prominent role for ENSO in the Millennium Drought [*van Dijk et al.*, 2013; *Verdon-Kidd and Kiem*, 2009], with additional influences from the Southern Annular Mode [*Verdon-Kidd and Kiem*, 2009] and the IPO [*van Dijk et al.*, 2013]. In contrast, the extreme pluvial in 2011 was forced primarily by a large La Niña event [*Cai and van Rensch*, 2012; *Evans and Boyer-Souchet*, 2012; *Lewis and Karoly*, 2015], with additional contributions from negative phases of the IPO [*Cai and van Rensch*, 2012] and IOD [*Verdon-Kidd et al.*, 2014] and a strong positive departure in the Southern Annular Mode [*Timbal and Fawcett*, 2012].

While their genesis was clearly natural, the extreme nature of these events has motivated investigations into a possible role for anthropogenic climate change. For the Millennium Drought, several studies [*Cai et al.*, 2009b; *Nicholls*, 2004; *Ummenhofer et al.*, 2009] concluded that extreme temperatures increased evaporative demand, amplifying surface drying beyond what would have occurred from the (natural) sea surface temperature (SST) induced rainfall deficits alone. Some have concluded, however, that the high temperature anomalies were instead a response to the drought, rather than a contributing factor [*Lockart et al.*, 2009]. Other studies suggest that the precipitation deficits themselves during the drought were possibly influenced by long-term, anthropogenically-driven drying trends caused by poleward storm track shifts and the intensification and expansion of the subtropical dry zone in the Southern Hemisphere [*Cai et al.*, 2014; *Post et al.*, 2014; *Theobald et al.*, 2015; *Verdon-Kidd et al.*, 2014]. Analyses of the 2010-2011 summer have also found evidence for an anthropogenic effect on the floods and extreme rainfall from elevated SSTs [*Evans and Boyer-Souchet*, 2012; *Hendon et al.*, 2014; *Ummenhofer et al.*,

2015], although some of these results may be model dependent [*Lewis and Karoly*, 2015].

The Millennium Drought and 2011 pluvial were extreme, but understanding the anthropogenic climate change contribution to these events requires a more complete sampling of the range of natural climate variations than is available from the short instrumental record. This has motivated the development of several paleoclimate reconstructions to extend the climate record of eastern Australia further back in time. One of the first to specifically address the issue of the Millennium Drought was the streamflow reconstruction of *Gallant and Gergis* [2011] for the River Murray. They concluded that streamflow deficits during the Millennium Drought were a 1-in-1500 year event, the driest period back to 1783. This conclusion was further supported by the *Gergis et al.* [2012] precipitation reconstruction for southeastern Australia, where the authors determined, with a >97% likelihood, that 1998–2008 was the driest decade in the region since initial European settlement in 1788. Two recent reconstructions, however, point to much larger natural variability in hydroclimate in centuries prior to the historical period. *Ho et al.* [2015] developed a rainfall reconstruction for the Murray-Darling Basin and found multiple instances of decadal length dry and wet periods over the last two millennia that exceeded any event in the instrumental record. *Vance et al.* [2015], in a millennial length IPO reconstruction from the Law Dome ice core, similarly identified periods of persistent drought in eastern Australia over the past millennium, including exceptional aridity during the 1100s. Notably, reconstructions of precipitation over southwestern Australia suggest that some of these periods of prolonged aridity may have even extended across the entire southern half of the continent [*Cullen and Grierson*, 2009].

There are thus still considerable uncertainties regarding how the Millennium Drought

and 2011 pluvial compare to natural hydroclimate variations over recent centuries, especially in a broader spatiotemporal context. Here, we build on previous work by conducting a new analysis of the Australia-New Zealand Drought Atlas (ANZDA), an annually and spatially resolved proxy (tree-rings and corals) reconstruction of hydroclimate variability for eastern Australia, Tasmania, and New Zealand [*Palmer et al.*, 2015]. Combined with climate model projections from Phase 5 of the Coupled Model Intercomparison Project [CMIP5; *Taylor et al.*, 2012], we investigate the past context and future trajectory of extreme hydroclimate events in eastern Australia. Specifically, we focus on two research questions: 1) How do the Millennium Drought and 2011 pluvial compare to the full range of drought variability over the last 500 years, as represented in the ANZDA? and 2) How will the probability of similar events shift with climate change over the 21$^{st}$ century?

## 2. Materials and Methods

### 2.1. The Australia-New Zealand Drought Atlas (ANZDA)

The ANZDA [*Palmer et al.*, 2015] is a gridded (0.5$^{o}$ spatial resolution), annually resolved reconstruction of austral summer self-calibrating Palmer Drought Severity Index [PDSI; *Palmer*, 1965]. The year is centered on January so that, for example, values for 2011 represent the average of December 2010, January 2011, and February 2011. PDSI is a normalized indicator of drought, using a soil moisture bucket model to simultaneously track changes in moisture supply (precipitation) and demand (evapotranspiration) from month to month. PDSI integrates changes in the surface moisture balance over a timescale of approximately 12 months [*Guttman*, 1998] and compares well with more sophisticated soil moisture models [e.g., *Cook et al.*, 2015; *Williams et al.*, 2015]. The DJF PDSI used in our analysis of Australian hydroclimate thus differs from other drought indicators (e.g.,

precipitation, streamflow) in terms of 1) the aspect of the hydrologic cycle it most closely represents (soil moisture) and 2) its inherent seasonality (likely biased towards spring and summer, while still incorporating climate information from previous seasons). It is expected, therefore, that results and conclusions drawn from analyses of PDSI may differ from studies targeting other hydroclimatic variables [e.g., *Gallant and Gergis*, 2011; *Gergis et al.*, 2012]. Positive values of PDSI indicate wetter than normal conditions (pluvials), while negative values indicate drier than normal conditions (droughts). PDSI is widely used as a paleoclimate reconstruction target [*Cook et al.*, 2004, 2010; *Smerdon et al.*, 2015] and in observational [e.g., *van der Schrier et al.*, 2013] and model-based [e.g., *Cook et al.*, 2014] analyses of drought dynamics.

While different from what may be considered more standard hydroclimate variables (e.g., precipitation anomalies, streamflow deficits), summer-season PDSI is a valuable drought indicator in many regions, including eastern Australia. PDSI integrates climate across multiple months and seasons, providing a longer-term view of moisture deficits and surpluses than can be derived from monthly precipitation anomalies alone, and incorporates information on both moisture supply and demand, representing a more complete picture of the surface moisture balance. This is especially critical for analyzing climate change impacts on drought, which are expected to arise from shifts in both precipitation and evaporative demand [e.g., *Cook et al.*, 2014, 2015; *Scheff and Frierson*, 2013; *Williams et al.*, 2015]. More specifically for southeastern Australia, summer PDSI is an indicator of initial soil moisture conditions for the winter cropping season. The impacts of insufficient precipitation during the growing season and at the start of the cropping season are exacerbated by a preceding dry summer, especially in areas that practice minimal tillage

farming and sow before the autumn breaking rains [*Pook et al.*, 2006]. Fire risks across large areas of arid and semi-arid Australia are also influenced by low soil moisture levels that increase the ability for fuel to burn and can also temporarily increase litter fall from vegetation, further increasing fuel loads [*Bradstock*, 2010]. Because of its warm season bias, summer PDSI can also be a good proxy for extreme rainfall and flooding, especially for summer-dominated rainfall regions (e.g., northern Australia) where these events can be devastating [*Holmes*, 2012].

The ANZDA reconstruction (1500–2012) is based on a network of 176 drought-sensitive tree-ring chronologies and one coral luminescence proxy series. PDSI values in the ANZDA from 1500–1975 are derived from the proxy network, and merged with the underlying instrumental dataset [*van der Schrier et al.*, 2013] from 1976–2012. The leading principal component in the ANZDA explains $> 50\%$ of the underlying variance and is strongly correlated with the IPO [*Palmer et al.*, 2015]. The reconstruction validates well over eastern Australia and identifies droughts that are independently corroborated in other reconstructions and historical documents. Full details, including complete calibration and validation information, can be found in *Palmer et al.* [2015].

### 2.2. CMIP5 Simulations

To investigate climate change impacts on drought, we use PDSI calculated from CMIP5 model projections of the 21$^{st}$ century [available from `http://www.ldeo.columbia.edu/~jsmerdon/2014_clidyn_cooketal_supplement.html`; *Cook et al.*, 2014]. These projections cover the time interval 1901–2099, using the historical (1850–2005) and RCP 8.5 (2006–2099; business-as-usual, high greenhouse gas emissions) forcing scenarios. This ensemble includes projections from 15 models, several with multiple ensemble members, for

a total of 34 individual simulations. These model PDSI calculations use the physically based Penman-Monteith formulation for potential evapotranspiration (PET) [*Smerdon et al.*, 2015], incorporating model trends in temperature, humidity, and net radiation (the PDSI target field [*van der Schrier et al.*, 2013] for the ANZDA reconstruction also used Penman-Monteith). Because the Penman-Monteith formulation is a more physically based approximation of PET, it avoids the limitations of more simple PET methods (e.g., Thornthwaite) that overestimate temperature and PET-forced drought trends [e.g. *Hoerling et al.*, 2012]. We analyze DJF average PDSI from these projections for consistency with the ANZDA. Further details on these drought projections and PDSI calculations can be found in *Cook et al.* [2014], including global PDSI projections for each individual model.

### 2.3. Analyses

Prior to any analysis, PDSI data from the CMIP5 simulations and ANZDA at each grid point were recentered to a mean of zero over the 20$^{th}$ century (1901–2000). This ensures the same baseline average conditions for comparing drought variability across the reconstruction and model simulations. To identify regions for time series analysis, we first conducted a Principal Component Analysis (PCA) on the continental Australia portion of the ANZDA, retaining and rotating the first 3 modes using varimax rotation. The resulting three rotated modes account for 68.5% of the underlying variance with three primary centers of action (Figure 1). The first is over southeast Australia and the Murray-Darling Basin ('Southeastern Australia'; 138°-154°E, 28°-39.5°S). The second mode is focused to the west of the Great Dividing Range in Queensland ('Western Queensland'; 138°-145°E, 18°-28°S). The third and final principal component projects most strongly along

the coast of northeastern Australia ('Coastal Queensland'; 145°-154°E, 18°-28°S). Using the PCA analysis for guidance, we then spatially averaged PDSI over these regions from the ANZDA and CMIP5 model simulations to generate time series for analysis. Uncertainties in our reconstructed regional drought series are calculated as the 90$^{th}$ percentile prediction intervals, estimated from a linear regression between the tree-ring and instrumental PDSI from 1902–1929 (the independent validation interval used in the ANZDA reconstruction). To quantify drought risk, we empirically fit kernel densities (cumulative distribution functions) to these regional average PDSI distributions in the ANZDA and CMIP5 simulations. Comparisons between the fully reconstructed (1500–1975) and instrumental (1902–2012) PDSI showed no significant differences ($p > 0.05$) in either median PDSI (Wilcoxon rank-sum test) or dispersion (Ansari-Bradley test). To provide context for recent extreme hydroclimate events, we highlight, from the ANZDA record, previous extreme drought and pluvial years.

To compare and evaluate our results within the context of seasonal precipitation variability, we conducted two sets of comparisons between PDSI and precipitation. First, we calculated Spearman's rank correlations (1902–1929) between the PDSI (tree-ring reconstructed and instrumental) and single and cumulative season precipitation from the CRU 3.21 climate grids [*Harris et al.*, 2014]. These are the same precipitation data used in the construction of the instrumental PDSI [*van der Schrier et al.*, 2013] targeted in the ANZDA reconstruction. Second, we compare our reconstructed PDSI time series from Southeastern Australia to the historical precipitation reconstruction of *Ashcroft et al.* [2014]. This regional precipitation dataset consists of seasonal, standardized precipitation anomalies for 1860–2012, constructed from homogenized historical precipitation records

distributed across a region (136°–154°E and 26°–40°S) approximately equivalent to our defined Southeastern Australia region. For the *Ashcroft et al.* [2014] comparison, we calculate Spearman's rank correlations between seasonal precipitation and reconstructed PDSI for three intervals (1860–1901, 1902–1929, 1930–1975) and compare anomalies during the major multi-year historical drought events (Federation, World War II, Millennium). As with the PDSI from the ANZDA and CMIP5 simulations, we recentered these seasonal precipitation anomalies to a zero 20$^{th}$ century mean prior to any analyses.

Aside from analyzing single-year droughts and pluvials in the reconstruction and CMIP5 simulations, we also target analogues for the Millennium Drought. We define our Millennium Drought analogues as 7-year running mean PDSI (in either the reconstruction or model ensemble) with a magnitude equal to or drier than the 7-year mean for the Millennium Drought (2003–2009). We acknowledge that this ignores situations where two dry 7-year analogues may overlap, or occur as part of the same persistent drought event. However, we use this as the most straightforward method for determining how the Millennium Drought compares to equivalent periods in the ANZDA, and how the risk of similar events may change under increased greenhouse gas forcing.

## 3. Results

### 3.1. The Millennium Drought and 2011 Pluvial

PDSI is primarily an indicator of soil moisture variability, integrated over multiple seasons. It is expected, then, that PDSI may record drought differently compared to variables that track other parts of the hydrologic cycle, such as precipitation or streamflow. Most studies based on precipitation deficits [e.g., *Ummenhofer et al.*, 2009] define the Millennium Drought from the mid-1990s to 2008 or 2009. In the ANZDA, average PDSI over all three

of our study regions in 2002 is −0.16, only slightly below normal. The following year is the first major and widespread year of drought in the dataset, with three-region average PDSI=−2.13. Given this, we therefore define the Millennium Drought from 2003–2009, acknowledging that analyses of other hydroclimatic variables may lead to different results and interpretations.

Drought conditions were most intense and widespread in the ANZDA in the first year (2003) of the Millennium Drought (Figure 2), covering most of eastern Australia from Tasmania to the Cape York Peninsula. By 2008 and 2009, conditions had either ameliorated or recovered across most of the continent except for some intensification in the south. The year 2011 was exceptionally wet over nearly all of eastern Australia (Figure 2), with grid cell values of PDSI in excess of +5 in all three regions. During 2011, values of area average PDSI were positive enough that all three regions qualified as "very wet" by the standard PDSI scaling definitions (`http://drought.unl.edu/Planning/Monitoring/ComparisonofIndicesIntro/PDSI.aspx`) (Western Queensland PDSI= +4.32, Coastal Queensland PDSI= +5.24, Southeastern Australia PDSI= +3.82).

### 3.2. Precipitation Seasonality in the ANZDA

Instrumental and reconstructed summer-season PDSI are mostly positively and significantly (one-sided test, $p \leq 0.05$) correlated with instrumental precipitation (Figure 3). The strongest single-season precipitation correlations are summer and antecedent spring, with weaker but mostly still significant correlations with antecedent winter and autumn. Both instrumental and reconstructed PDSI show small negative correlations with preceding single season autumn precipitation for Southeastern Australia. The presence of the negative correlation in the instrumental PDSI comparison indicates this is not an arti-

fact of the reconstruction process, and thus may reflect some biases or noise over this relatively short period (28 years) in the instrumental record. The cumulative seasonal correlation plots clearly show the important secondary influence of these previous seasons on the summer PDSI. In nearly all cases, instrumental PDSI correlations with cumulative precipitation from multiple seasons (e.g., SON+DJF) are stronger than any single-season, with the largest increase in correlation occurring when SON is combined with DJF. Seasonal correlation patterns for the reconstructed PDSI are similar (and $\geq +0.6$ for Coastal Queensland and Southeastern Australia), although the winter and autumn signals in the reconstructed PDSI are weaker in both the single and cumulative season cases. This likely reflects some additional biases in the underlying proxies towards spring and summer (beyond those embedded in the PDSI calculation), or potential non-PDSI related variability in the proxies themselves.

The reconstructed PDSI is also positively and significantly correlated with the *Ashcroft et al.* [2014] historical precipitation reconstruction over Southeastern Australia (Figure 4). Correlations with cumulative season precipitation are similar, or even slightly higher, during the ANZDA verification interval (1902–1929) compared to the later calibration period (1930–1975), though they are substantially lower during the late 19$^{th}$ century (1860–1901). Proxy availability in the reconstruction, however, is nearly uniform over the entire period, suggesting the decreased correlation strength may instead reflect changes in the earliest precipitation records used in the historical precipitation reconstruction. Indeed, the network of stations in the *Ashcroft et al.* [2014] reconstruction for the late 19$^{th}$ century increases from less than 20 in 1860 to over 40 in 1900 [Figure 3, *Gergis and Ashcroft*, 2013]. Regardless, correlations with the ANZDA are mostly significant in all seasons for

all intervals, with the strongest relationship between summer PDSI and cumulative spring and summer precipitation, a result consistent with the previous CRU precipitation analysis. Combined with the instrumental analysis, these results demonstrate the ability of the reconstructed PDSI to capture a substantial fraction of the cumulative season precipitation variability in all three regions.

Differences in the magnitude of the precipitation and PDSI anomalies are apparent across the three major multi-year historical era droughts (Figure 5). Autumn precipitation deficits were the main driver of the Millennium Drought [e.g., *Timbal and Fawcett*, 2013] with secondary contributions from more modest deficits in the winter and spring. This is confirmed in the *Ashcroft et al.* [2014] reconstruction, which shows autumn precipitation deficits during the Millennium Drought were the largest single-season precipitation anomalies across these three events. Summer season PDSI in the ANZDA, however, was slightly drier during the WWII drought compared to the Millennium Drought, which can likely be explained in terms of the precipitation seasonality in the ANZDA. As noted, the sensitivity of the summer season PDSI to autumn precipitation is weaker than for the other three seasons, which suggests that the ANZDA may underestimate the magnitude of the Millennium Drought. The WWII drought, however, was forced by the single largest SON precipitation deficit across the three events, a season that is strongly correlated with summer season PDSI and an event that the ANZDA is well suited to capture. This again highlights the seasonal biases in the ANZDA summer PDSI, and indicates the need for caution when interpreting and drawing conclusions about hydroclimate events expressed across different drought indicators and variables.

### 3.3. Hydroclimate Variability Over the Last 500 Years

The last 500 years of hydroclimate variability are shown for our three regions combined (Figure 6) and individually (Figure 7). Over the ANZDA verification interval (1902–1929), the instrumental and reconstructed PDSI correlate significantly (Spearman's rank correlations): $\rho = 0.587$ in Western Queensland, $\rho = 0.707$ in Coastal Queensland, $\rho = 0.510$ in Southeastern Australia, and $\rho = 0.641$ for all three regions combined. This level of skill is comparable to the precipitation reconstruction of *Gergis et al.* [2012] (verification period correlations between 0.41 to 0.70; their Tables 4 and 5) and the streamflow reconstruction of *Gallant and Gergis* [2011] (verification period correlations between 0.46 to 0.70; their Table 4). The interannual variability in drought area ($PDSI < 0$; Figure 6, bottom panel) is high, a pattern exemplified by the recent extreme events that are the focus of this study. The multi-year average drought area for the Millennium Drought (2003–2009; red dashed line) covered 81.4% of eastern Australia, with 2003 appearing as the driest year of this drought in terms of PDSI anomaly (−2.13) and among the top ten most widespread (98.5% drought area) drought years since at least 1500 CE. Similarly, exceptional wetness was widespread across eastern Australia in 2011 (blue dashed line), with only 1.3% of the area in drought during this time. The regional ANZDA time series (Figure 7) clearly identify major historical droughts that occurred outside the reconstruction calibration interval (1930–1975), including the well-documented Federation Drought (1895–1902) and the Settlement Drought of 1791–1792. Other periods of enhanced aridity in the ANZDA are corroborated by other reconstructions [*Ho et al.*, 2015], including the early 1500s, late 1700s, and 1820s to 1840s. From a summer PDSI perspective, 2011 (dashed blue line, Figures 6 and 7) stands out as exceptionally wet. Multi-year mean PDSI during the

Millennium Drought (dashed brown line, Figures 6 and 7), however, appears to fall well within the range of variability (and uncertainties) in the reconstruction.

Nominally, the driest year of the Millennium Drought in each region was 2003, and the driest single years in the record were 1519 (Coastal Queensland), 1565 (Western Queensland), and 1839 (Southeastern Australia) (Figure 8). The Settlement Drought (1792) was also notable and appears as a significant event in the ANZDA, ranking in the top five driest for Southeastern Australia and Coastal Queensland. This drought had major impacts in New South Wales, causing a partial failure of the wheat harvest and threatening the water supply in Sydney [*Russell*, 1877], and occurred in conjunction with a large El Niño [*Li et al.*, 2013] that also caused significant drought in South Asia [*Grove*, 1998] during the same year (note, though, some overlap in the proxies used in the ANZDA and the *Li et al.* [2013] ENSO reconstruction).

The 7-year average PDSI for the Millennium Drought (2003–2009) does not rank as exceptionally dry in any region when compared to all other possible 7-year running mean PDSI values in the ANZDA. As noted previously, this is likely due, at least in part, to the fact that the Millennium Drought was primarily driven by precipitation deficits during the autumn, the season with the weakest signal in the ANZDA. In all three regions, the driest 7-year running mean PDSI occurred during the 16$^{th}$ century (Figure 9). This includes two extremely dry 7-year periods in the early 1500s that were part of a persistent, multi-decadal drought event in all three regions. To quantify this event, we use a simple criteria [described in *Coats et al.*, 2013, 2015] where multi-year drought events are defined as starting with two consecutive dry years (PDSI$<0$) and ending with two consecutive wet years (PDSI$\geq 0$) ("two-start two-end"; 2S2E). By this metric, the early 1500s drought is

the longest in all three regions: 1500–1522 (23 years) in Western Queensland, 1500–1527 (28 years) in Coastal Queensland, and 1500–1522 (23 years) in Southeastern Australia.

Compared to the ANZDA reconstructed PDSI (1500–1975), 2011 is the wettest single year for all three regions. When comparing across the instrumental PDSI dataset (1902–2012), however, 1974 is nominally the wettest in both Western Queensland and Southeastern Australia, while 2011 remains the wettest in Coastal Queensland. Other major wet years in the ANZDA (Figure 10) include 1572 and 1573, both major La Niña events in the reconstruction of *Li et al.* [2013], ranking among the top six wettest years in all three regions. Despite differences in ranking for 1974 between the instrumental and reconstructed PDSI, reconstructed PDSI for 1974 and 1976 are both still exceptionally wet in Western Queensland and Southeastern Australia, ranking among the top five wettest years for both regions. These relatively wet conditions in the 1970s coincided with multi-year flooding of Lake Eyre [*Allan*, 1985] and may have contributed, at least in part, to the over-allocation of water resources in subsequent decades [*Quiggin*, 2001; *Wei et al.*, 2011; *Young and McColl*, 2003].

For most of these events in the ANZDA, it is difficult to assign exact ranks with statistical confidence because of the significant overlap in the error estimates (i.e., shaded blue regions, Figures 6 and 7). In light of this, rankings of most dry and wet years in the ANZDA are best interpreted more generally, rather than in terms of their exact position relative to other years. However, the most extreme wet years in the instrumental and reconstructed PDSI (1974 in Western Queensland and Southeastern Australia, 2011 in Coastal Queensland) do stand apart, even when accounting for uncertainty in the reconstruction. We calculate for how many years instrumental PDSI values for 1974 in Western

Queensland and Southeastern Australia and 2011 in Coastal Queensland fall outside the upper prediction interval for the reconstruction (1500–1975). This represents, effectively, a one-tailed test ($p \leq 0.05$) of the null hypothesis that these years are NOT the wettest in the record. PDSI in 1974 falls outside the confidence interval in 432 of 476 reconstructed years (90.8% of years) for Southeastern Australia and 457 of 476 reconstructed years (96.0% of years) in Western Queensland, making it likely that 1974 was the wettest event in these regions. For Coastal Queensland, 2011 stands out as even more extreme. PDSI values for 2011 in this region fall outside the upper prediction interval in 464 of the 476 reconstructed years ($> 97\%$ of years). This translates to only 12 years in the entire reconstruction that may have been wetter than 2011 in Coastal Queensland, given the uncertainties in the reconstruction. From this, we conclude that 2011 was likely the wettest summer in Coastal Queensland back to 1500 CE.

### 3.4. CMIP5 PDSI Projections

For 1902–1975, we compared the cumulative probability distributions of instrumental PDSI, reconstructed PDSI, and PDSI calculated from the multi-model CMIP5 ensemble (Figure 11, left column). For all comparisons (observed versus reconstructed PDSI, observed versus CMIP5 PDSI, reconstructed versus CMIP5 PDSI), we found no significant differences in the underlying distributions (two-sided Kolmogorov-Smirnov test, $p > 0.05$) indicating, at least in aggregate, that the CMIP5 ensemble adequately captures the observed and reconstructed hydroclimate variability over this interval. We also compared the frequency (Figure 11, center column) of major drought ($PDSI \leq -1$) and pluvial years ($PDSI \geq +1$) for each individual model simulation (box and whisker plots) and the instrumental (red dots) and reconstructed (green dots) PDSI. Both observed and re-

constructed drought and pluvial frequencies fall within the range of the CMIP5 ensemble, with largest differences in Western Queensland where the models and reconstructed PDSI diverge most strongly from the observations. It is difficult to know, however, whether these disagreements arise from biases related to the fewer number of years in the observed and reconstructed PDSI relative to the large CMIP5 ensemble. Finally, we compare the frequencies of droughts of different length between the models and reconstruction using the 2S2E criterion discussed previously (Figure 11, right column). To best sample the longest drought events, here we calculate the distributions for the full ANZDA (1500–2012) and from the CMIP5 ensemble for 1901–2012 (i.e., before the major greenhouse gas forced signal in these simulations emerges). Overall, the models generally simulate fewer long-term droughts than the ANZDA reconstruction, especially in Western Queensland and Southeastern Australia.

For the latter half of the 21$^{st}$ century (2050–2099, RCP 8.5 scenario), the general model consensus over eastern Australia is for a shift towards more negative mean PDSI values, indicative of drier average conditions relative to the 20$^{th}$ century (Figure 12). Cross-model consistency is generally larger for Southeastern Australia, with only a subset of models (CanESM2, CCSM4, CNRM-CM5, MIROC5, NorESM1-M) suggesting a tendency for wetting in any region. Among the models in our full ensemble, only three (MIROC-ESM-Chem, MIROC-ESM and GISS-E2-R) were considered 'poor' performers in a recent validation study of the CMIP5 models for Australia [*Moise et al.*, 2015].

To identify the relative contributions of different processes (precipitation or PET) to this drying trend, we calculated alternate versions of the PDSI in which trends in either precipitation or PET over the 21$^{st}$ century were removed. Precipitation-induced de-

clines in PDSI (Figure 13, blue lines) are small in Coastal Queensland (2050–2099, mean PDSI= −0.28) and near zero in Southeastern Australia (PDSI= −0.07) and Western Queensland (PDSI= +0.01). Including the effects of changing PET (forced by trends in temperature, humidity, and net radiation) leads to more consistent and substantial drying in all regions (Figure 13, red lines), with the largest amplification in Coastal Queensland (PDSI= −1.00) and Southeastern Australia (PDSI= −1.18). Increases in PET are due primarily to warming-induced increases in the vapor pressure deficit, with secondary contributions from overall increases in surface energy availability. These mechanisms are described in more detail in *Cook et al.* [2014] and other studies [e.g., *Scheff and Frierson*, 2013].

We compared PDSI distributions from the ANZDA (1500–2012) against three intervals from our multi-model ensemble: 1901–2000, 2020–2049, and 2050–2099 (Figure 14). The model distributions incorporate model trends in both precipitation and PET. The progressive drying in the model ensemble from the 20$^{th}$ century to the end of the 21$^{st}$ century is clearly apparent and, with this drying, the risk of annual PDSI values equal to or drier than the worst drought years in the ANZDA increases substantially. This corresponds to a future risk in different regions of 5% (1565, Western Queensland; 1519, Coastal Queensland), and 7% (1833, Southeastern Australia), well above the baseline estimates (< 1% risk) in the ANZDA. Somewhat paradoxically, the probability of extreme wet years of equal or greater magnitude to 2011 also increases under a scenario of progressive 21$^{st}$ century drying. The likelihood of an extreme event equivalent to or wetter than 2011 increases to 1% (Western Queensland), 0.5% (Coastal Queensland), and 0.6% (Southeastern Australia). While small in absolute terms, the increased risk is relatively large given

the exceptionally low likelihood in the ANZDA. An increase in extreme wet years may seem counter-intuitive given the mean drying in the PDSI distributions, but this result is generally consistent with the expected response of extreme precipitation and floods to warming [e.g., *Easterling et al.*, 2000; *Trenberth*, 2011; *Trenberth et al.*, 2015]. This was evident in the 2010–2011 summer, when exceptionally warm SSTs around northern Australia fueled enhanced onshore moisture transport [*Evans and Boyer-Souchet*, 2012; *Ummenhofer et al.*, 2015]. Even with these increases in likelihood of wet extremes, however, pluvial years analogous to 2011 are likely to remain exceptionally rare.

We conduct a similar analysis in the CMIP5 ensemble for analogues of the Millennium Drought and the driest 7-year periods in the ANZDA (Figure 15). As with the single year events (Figure 14), the risk of 7-year mean PDSI values equal to or drier than the Millennium Drought increases markedly. For Coastal Queensland and Southeastern Australia, where the Millennium Drought was most strongly expressed, the risk of a similar run of 7-year PDSI increases from $\leq 10\%$ in the ANZDA to 39% (Coastal Queensland) or 49% (Southeastern Australia) during 2050–2099. Similarly, the risk of 7-year running mean PDSI equal to or drier than the driest 7-year periods increases to $> 15\%$ in Western Queensland and Coastal Queensland and $> 25\%$ in Southeastern Australia. This indicates that the likelihood of eastern Australia experiencing a 7-year period of summer drought similar to the Millennium Drought increases substantially by the end of the 21$^{st}$ century, under a scenario of continued high levels of greenhouse gas emissions.

## 4. Discussion and Conclusions

Attribution of climate extremes is a rapidly advancing field of research, especially for hydroclimate events such as floods and droughts [*Trenberth et al.*, 2015]. But one major

limitation is the relatively short duration of the instrumental record, which can make it difficult to confidently characterize the full range of natural climate variability. Here, we use the ANZDA and projections from the CMIP5 archive to investigate how two recent extreme hydroclimate events in Australia [e.g., *Cai et al.*, 2009b; *Evans and Boyer-Souchet*, 2012; *Hoerling et al.*, 2014; *Nicholls*, 2004; *Ummenhofer et al.*, 2009, 2015] compare to the last 500 years of natural variability and how their likelihood may shift with increased greenhouse gas forcing.

Neither the single most extreme year of the Millennium Drought (2003) or the 7-year mean PDSI from 2003–2009 appear as unusually severe relative to the last 500 years of natural variability in the ANZDA. Recurrent periods of extreme and persistent drought are apparent in the ANZDA prior to the observational record, consistent with other largely independent reconstructions of hydroclimate for the region [*Ho et al.*, 2015; *Vance et al.*, 2015]. Of note, the ANZDA shows a rather exceptional period of multi-decadal drought across eastern Australia in the early 1500s, the most persistent multi-year drought event of the last 500 years. As noted, however, the error estimates in the reconstruction time series are too large to quantitatively and definitively assign ranks for most events. An exception is the extreme pluvial during 2011 over Coastal Queensland, which stands (in terms of summer season PDSI) as nominally the single wettest year in the observational record and reconstruction. This year is a full +1.4 PDSI units wetter than the second wettest year in the reconstruction (1572), and only 12 of the 476 reconstructed years have upper confidence limits exceeding 2011. Viewed probabilistically, this equates to 2011 exceeding 97% of the reconstructed values after taking into account their estimated uncertainties. In light of this result, we conclude that 2011 was likely the wettest summer of the last

500 years in Coastal Queensland, though other years were likely wetter in other parts of Queensland and Southeastern Australia. Comparing against an ensemble of climate projections for the 21st century, average conditions in eastern Australia are expected to become drier in the latter half of the 21st century, with amplified risk of both dry and wet extremes of similar intensity to the Millennium Drought and 2011 pluvial.

Our findings and conclusions regarding these recent events are very likely sensitive to the seasonal precipitation biases in the underlying ANZDA reconstruction. As demonstrated, the summer season PDSI in the ANZDA is most sensitive to summer and antecedent spring precipitation. The ANZDA therefore likely underestimates the severity of the Millennium Drought, which was forced by autumn precipitation deficits that are only weakly and insignificantly expressed in this drought reconstruction. Indeed, independent reconstructions of streamflow [e.g., *Gallant and Gergis*, 2011] and precipitation [e.g., *Gergis et al.*, 2012] for eastern Australia confirm the exceptional nature of the Millennium Drought. Conversely, the ANZDA is well suited for evaluation of the 2011 pluvial event, which was forced by extreme summer precipitation.

The PDSI projections in the CMIP5 models have their own set of uncertainties, foremost of which are the structural uncertainties in the models themselves. To address this, we have presented results from each individual model and ensemble member (Figure 12) and used the full multi-model ensemble in our kernel density functions and drought risk analysis. Other studies have criticized PDSI as an overly simplistic drought metric that may overestimate drying trends in response to climate change [e.g., *Hoerling et al.*, 2012; *Burke*, 2011]. One often-highlighted weakness is the absence of an atmospheric carbon dioxide effect on plant physiology in the standard PDSI calculation, which would be ex-

pected to dampen PET-induced drying [e.g., *Roderick et al.*, 2015]. We consider, however, that PDSI is still a useful and reasonable metric for connecting drought information in the paleoclimate record with model projections. This is supported by the similarities in the 20$^{th}$ century ANZDA and CMIP5 reconstructions (Figure 11), and the general good consistency between PDSI and more complex models of soil moisture for both past and future time intervals found in other studies [*Cook et al.*, 2015; *Smerdon et al.*, 2015; *Williams et al.*, 2015]. Further, there is emerging evidence that the moisture-savings benefits of enhanced carbon dioxide concentrations may be overstated [*Frank et al.*, 2015; *Ukkola et al.*, 2016], especially in land surface and vegetation models [*De Kauwe et al.*, 2013; *Kolby Smith et al.*, 2015]. Finally, we note that the importance of warming and PET as the dominant drying mechanisms in the CMIP5 projections is consistent with recent arguments made for anthropogenic amplification of the Millennium Drought [*Cai et al.*, 2009b; *Nicholls*, 2004; *Ummenhofer et al.*, 2009].

The Millennium Drought was a prolonged disaster in eastern Australia, with significant agricultural and economic impacts [*van Dijk et al.*, 2013; *Heberger*, 2011]. Beyond the extreme autumn precipitation deficits, however, the impacts and perception of this drought may have been amplified by other factors. *Saft et al.* [2015], for example, noted that streamflow deficits during the drought were more severe than would have been predicted from precipitation anomalies alone, likely a consequence of climatic and landscape factors. Perceptions may have been further influenced because this drought occurred after an extended period of above-average moisture availability in the decades following the World War II drought. The subsequent period of rapid expansion of agriculture and water resource exploitation in the region may have set unrealistic expectations for moisture

availability [*Musgrave*, 2008]. This was followed by a late 20$^{th}$ century declining trend in autumn rainfall associated with the weather systems most responsible for moisture supply at the start of the winter growing season in southeast Australia [*Pook et al.*, 2009], leading directly into the Millennium Drought. Regardless, the ANZDA suggests that summer-season soil moisture deficits similar to what occurred during the Millennium Drought are not uncommon. These results therefore provide strong motivation for policies that will increase resilience given the high likelihood of similar events occurring over the next century from both natural variations and anthropogenic forcing.

**Acknowledgments.** CSMT thanks the Australian Research Council for the provision of a Laureate Fellowship. Support was provided by the Australian Research Council through grants: FL100100195, LP120100310 and DP130104156 to CSM Turney and DP0878744, DP120104320, LP120200811, FT120100715 for PJ Baker. BI Cook supported by NASA. The ANZDA is freely available from the NOAA Paleoclimate Archive (`https://www.ncdc.noaa.gov/data-access/paleoclimatology-data/datasets`). Thanks to David Karoly and two anonymous reviewers for providing comments that greatly approved the quality of this manuscript. The authors also thank Linden Ashcroft, for providing the extended precipitation record for Southeastern Australia and additional valuable comments. Lamont contribution #.

## References


Allan, R. J. (1985), *The Australasian summer monsoon, teleconnections, and flooding in the Lake Eyre basin*, Royal Geographical Society of Australasia, SA Branch.

Ashcroft, L., D. J. Karoly, and J. Gergis (2014), Southeastern Australian climate variability 1860–2009: a multivariate analysis, *International Journal of Climatology*, *34*(6), 1928–1944, doi:10.1002/joc.3812.

Australian Bureau of Meteorology (2011), Australian Climate Variability and Change — Time Series Graphs, *website*.

Boening, C., J. K. Willis, F. W. Landerer, R. S. Nerem, and J. Fasullo (2012), The 2011 La Niña: So strong, the oceans fell, *Geophysical Research Letters*, *39*(19), n/a–n/a, doi:10.1029/2012GL053055.

Bradstock, R. A. (2010), A biogeographic model of fire regimes in Australia: current and future implications, *Global Ecology and Biogeography*, *19*(2), 145–158, doi:10.1111/j.1466-8238.2009.00512.x.

Burke, E. J. (2011), Understanding the Sensitivity of Different Drought Metrics to the Drivers of Drought under Increased Atmospheric CO2, *Journal of Hydrometeorology*, *12*(6), 1378–1394, doi:10.1175/2011JHM1386.1.

Cai, W., and P. van Rensch (2012), The 2011 southeast Queensland extreme summer rainfall: A confirmation of a negative Pacific Decadal Oscillation phase?, *Geophysical Research Letters*, *39*(8), n/a–n/a, doi:10.1029/2011GL050820.

Cai, W., T. Cowan, and M. Raupach (2009a), Positive Indian Ocean Dipole events precondition southeast Australia bushfires, *Geophysical Research Letters*, *36*(19), n/a–n/a, doi:10.1029/2009GL039902.

Cai, W., T. Cowan, P. Briggs, and M. Raupach (2009b), Rising temperature depletes soil moisture and exacerbates severe drought conditions across southeast australia, *Geophysical Research Letters*, *36*(21), n/a–n/a, doi:10.1029/2009GL040334.

Cai, W., P. van Rensch, T. Cowan, and A. Sullivan (2010), Asymmetry in ENSO Teleconnection with Regional Rainfall, Its Multidecadal Variability, and Impact, *Journal of Climate*, *23*(18), 4944–4955.

Cai, W., P. van Rensch, T. Cowan, and H. H. Hendon (2011), Teleconnection Pathways of ENSO and the IOD and the Mechanisms for Impacts on Australian Rainfall, *Journal of Climate*, *24*(15), 3910–3923, doi:10.1175/2011JCLI4129.1.

Cai, W., A. Purich, T. Cowan, P. van Rensch, and E. Weller (2014), Did Climate Change–Induced Rainfall Trends Contribute to the Australian Millennium Drought?, *Journal of Climate*, *27*(9), 3145–3168, doi:10.1175/JCLI-D-13-00322.1.

Coats, S., J. E. Smerdon, R. Seager, B. I. Cook, and J. F. González-Rouco (2013), Megadroughts in Southwestern North America in ECHO-G Millennial Simulations and Their Comparison to Proxy Drought Reconstructions*, *Journal of Climate*, *26*(19), 7635–7649, doi:10.1175/JCLI-D-12-00603.1.

Coats, S., J. E. Smerdon, B. I. Cook, and R. Seager (2015), Are Simulated Megadroughts in the North American Southwest Forced?, *Journal of Climate*, *28*(1), 124–142, doi:10.1175/JCLI-D-14-00071.1.

Cook, B. I., J. E. Smerdon, R. Seager, and S. Coats (2014), Global Warming and 21st century drying, *Climate Dynamics*, *43*(9-10), 2607–2627, doi:10.1007/s00382-014-2075-y.

Cook, B. I., T. R. Ault, and J. E. Smerdon (2015), Unprecedented 21st century drought risk in the American Southwest and Central Plains, *Science Advances*, *1*(1), doi:10.

1126/sciadv.1400082.

Cook, E. R., C. A. Woodhouse, C. M. Eakin, D. M. Meko, and D. W. Stahle (2004), Long-Term Aridity Changes in the Western United States, *Science*, *306*(5698), 1015–1018, doi:10.1126/science.1102586.

Cook, E. R., K. J. Anchukaitis, B. M. Buckley, R. D. D'Arrigo, G. C. Jacoby, and W. E. Wright (2010), Asian Monsoon Failure and Megadrought During the Last Millennium, *Science*, *328*(5977), 486–489, doi:10.1126/science.1185188.

Cullen, L. E., and P. F. Grierson (2009), Multi-decadal scale variability in autumn-winter rainfall in south-western Australia since 1655 AD as reconstructed from tree rings of Callitris columellaris, *Climate Dynamics*, *33*(2), 433–444, doi:10.1007/s00382-008-0457-8.

De Kauwe, M. G., B. E. Medlyn, S. Zaehle, A. P. Walker, M. C. Dietze, T. Hickler, A. K. Jain, Y. Luo, W. J. Parton, I. C. Prentice, B. Smith, P. E. Thornton, S. Wang, Y.-P. Wang, D. Warlind, E. Weng, K. Y. Crous, D. S. Ellsworth, P. J. Hanson, H. Seok Kim, J. M. Warren, R. Oren, and R. J. Norby (2013), Forest water use and water use efficiency at elevated CO2: a model-data intercomparison at two contrasting temperate forest FACE sites, *Global Change Biology*, *19*(6), 1759–1779, doi:10.1111/gcb.12164.

Easterling, D., J. Evans, P. Groisman, T. Karl, K. Kunkel, and P. Ambenje (2000), Observed Variability and Trends in Extreme Climate Events: A Brief Review, *Bulletin of the American Meteorological Society*, *81*(3), 417–425.

Evans, J. P., and I. Boyer-Souchet (2012), Local sea surface temperatures add to extreme precipitation in northeast Australia during La Niña, *Geophysical Research Letters*, *39*(19), n/a–n/a, doi:10.1029/2012GL052014.

Fasullo, J. T., C. Boening, F. W. Landerer, and R. S. Nerem (2013), Australia's unique influence on global sea level in 2010–2011, *Geophysical Research Letters*, *40*(16), 4368–4373, doi:10.1002/grl.50834.

Frank, D. C., B. Poulter, M. Saurer, J. Esper, C. Huntingford, G. Helle, K. Treydte, N. E. Zimmermann, G. H. Schleser, A. Ahlstrom, P. Ciais, P. Friedlingstein, S. Levis, M. Lomas, S. Sitch, N. Viovy, L. Andreu-Hayles, Z. Bednarz, F. Berninger, T. Boettger, C. M. D/'Alessandro, V. Daux, M. Filot, M. Grabner, E. Gutierrez, M. Haupt, E. Hilasvuori, H. Jungner, M. Kalela-Brundin, M. Krapiec, M. Leuenberger, N. J. Loader, H. Marah, V. Masson-Delmotte, A. Pazdur, S. Pawelczyk, M. Pierre, O. Planells, R. Pukiene, C. E. Reynolds-Henne, K. T. Rinne, A. Saracino, E. Sonninen, M. Stievenard, V. R. Switsur, M. Szczepanek, E. Szychowska-Krapiec, L. Todaro, J. S. Waterhouse, and M. Weigl (2015), Water-use efficiency and transpiration across European forests during the Anthropocene, *Nature Climate Change*, *5*(6), 579–583, doi:10.1038/nclimate2614.

Gallant, A. J. E., and J. Gergis (2011), An experimental streamflow reconstruction for the River Murray, Australia, 1783–1988, *Water Resources Research*, *47*(12), n/a–n/a, doi:10.1029/2010WR009832.

Gergis, J., and L. Ashcroft (2013), Rainfall variations in south-eastern Australia part 2: a comparison of documentary, early instrumental and palaeoclimate records, 1788–2008, *International Journal of Climatology*, *33*(14), 2973–2987, doi:10.1002/joc.3639.

Gergis, J., A. Gallant, K. Braganza, D. Karoly, K. Allen, L. Cullen, R. D'Arrigo, I. Goodwin, P. Grierson, and S. McGregor (2012), On the long-term context of the 1997–2009 'Big Dry' in South-Eastern Australia: insights from a 206-year multi-proxy rainfall reconstruction, *Climatic Change*, *111*(3-4), 923–944, doi:10.1007/s10584-011-0263-x.

671 Grove, R. H. (1998), Global impact of the 1789-93 El Nino, *Nature*, *393*(6683), 318–319,
672 doi:10.1038/30636.
673 Guttman, N. B. (1998), Comparing the Palmer Drought Index and the Standardized
674 Precipitation Index, *Journal of the American Water Resources Association*, *34*, 113–
675 121, doi:10.1111/j.1752-1688.1998.tb05964.x.
676 Harris, I., P. D. Jones, T. J. Osborn, and D. H. Lister (2014), Updated high-resolution
677 grids of monthly climatic observations –the CRU TS3.10 Dataset, *International Journal*
678 *of Climatology*, *34*(3), 623–642, doi:10.1002/joc.3711.
679 Heberger, M. (2011), *Australia's Millennium Drought: Impacts and Responses*, pp. 97–
680 125, Island Press/Center for Resource Economics, doi:10.5822/978-1-59726-228-6_5.
681 Hendon, H. H., E.-P. Lim, J. M. Arblaster, and D. L. T. Anderson (2014), Causes and
682 predictability of the record wet east Australian spring 2010, *Climate Dynamics*, *42*(5-6),
683 1155–1174, doi:10.1007/s00382-013-1700-5.
684 Ho, M., A. S. Kiem, and D. C. Verdon-Kidd (2015), A paleoclimate rainfall reconstruction
685 in the Murray-Darling Basin (MDB), Australia: 2. Assessing hydroclimatic risk using
686 paleoclimate records of wet and dry epochs, *Water Resources Research*, pp. n/a–n/a,
687 doi:10.1002/2015WR017059.
688 Hoerling, M. P., J. K. Eischeid, X.-W. Quan, H. F. Diaz, R. S. Webb, R. M. Dole,
689 and D. R. Easterling (2012), Is a Transition to Semipermanent Drought Conditions
690 Imminent in the U.S. Great Plains?, *Journal of Climate*, *25*(24), 8380–8386, doi:10.
691 1175/JCLI-D-12-00449.1.
692 Holmes, C. E. (2012), *Queensland Floods Commission of Inquiry: Final Report*, Queens-
693 land Floods Commission of Inquiry.

694 Horridge, M., J. Madden, and G. Wittwer (2005), The impact of the 2002–2003 drought
695 on Australia, *Journal of Policy Modeling*, *27*(3), 285 – 308, doi:http://dx.doi.org/10.
696 1016/j.jpolmod.2005.01.008, world Economy & European Integration.
697 Kiem, A. S., and S. W. Franks (2004), Multi-decadal variability of drought risk, eastern
698 Australia, *Hydrological Processes*, *18*(11), 2039–2050, doi:10.1002/hyp.1460.
699 Kiem, A. S., and D. C. Verdon-Kidd (2010), Towards understanding hydroclimatic change
700 in Victoria, Australia - preliminary insights into the "Big Dry", *Hydrology and Earth*
701 *System Sciences*, *14*(3), 433–445, doi:10.5194/hess-14-433-2010.
702 Kiem, A. S., S. W. Franks, and G. Kuczera (2003), Multi-decadal variability of flood risk,
703 *Geophysical Research Letters*, *30*(2), n/a–n/a, doi:10.1029/2002GL015992.
704 Kirby, M., R. Bark, J. Connor, M. E. Qureshi, and S. Keyworth (2014), Sustainable
705 irrigation: How did irrigated agriculture in Australia's Murray–Darling Basin adapt
706 in the Millennium Drought?, *Agricultural Water Management*, *145*, 154 – 162, doi:
707 http://dx.doi.org/10.1016/j.agwat.2014.02.013, exploring some of the socio-economic
708 realities of sustainable water management in irrigation.
709 Kolby Smith, W., S. C. Reed, C. C. Cleveland, A. P. Ballantyne, W. R. L. Anderegg,
710 W. R. Wieder, Y. Y. Liu, and S. W. Running (2015), Large divergence of satellite and
711 Earth system model estimates of global terrestrial CO2 fertilization, *Nature Climate*
712 *Change*, *advance online publication*, –, doi:doi:10.1038/nclimate2879.
713 Le Quéré, C., R. J. Andres, T. Boden, T. Conway, R. A. Houghton, J. I. House, G. Mar-
714 land, G. P. Peters, G. R. van der Werf, A. Ahlström, R. M. Andrew, L. Bopp, J. G.
715 Canadell, P. Ciais, S. C. Doney, C. Enright, P. Friedlingstein, C. Huntingford, A. K.
716 Jain, C. Jourdain, E. Kato, R. F. Keeling, K. Klein Goldewijk, S. Levis, P. Levy,

717 M. Lomas, B. Poulter, M. R. Raupach, J. Schwinger, S. Sitch, B. D. Stocker, N. Viovy,
718 S. Zaehle, and N. Zeng (2013), The global carbon budget 1959-2011, *Earth System*
719 *Science Data*, *5*(1), 165–185, doi:10.5194/essd-5-165-2013.

720 Lewis, S. C., and D. J. Karoly (2015), Are estimates of anthropogenic and natural influ-
721 ences on Australia's extreme 2010–2012 rainfall model-dependent?, *Climate Dynamics*,
722 *45*(3-4), 679–695.

723 Li, J., S.-P. Xie, E. R. Cook, M. S. Morales, D. A. Christie, N. C. Johnson, F. Chen,
724 R. D/'Arrigo, A. M. Fowler, X. Gou, and K. Fang (2013), El Nino modulations over the
725 past seven centuries, *Nature Climate Change*, *3*(9), 822–826, doi:10.1038/nclimate1936.

726 Lockart, N., D. Kavetski, and S. W. Franks (2009), On the recent warming in the Murray-
727 Darling Basin: Land surface interactions misunderstood, *Geophysical Research Letters*,
728 *36*(24), n/a–n/a, doi:10.1029/2009GL040598.

729 Moise, A., L. Wilson, M. Grose, P. Whetton, I. Watterson, J. Bhend, J. Bathols, L. Han-
730 son, T. Erwin, T. Bedin, et al. (2015), Evaluation of CMIP3 and CMIP5 Models over
731 the Australian Region to Inform Confidence in Projections, *Australian Meteorological*
732 *and Oceanographic Journal*, *65*(1), 19–53.

733 Musgrave, W. (2008), *Water policy in Australia: the impact of change and uncertainty*,
734 chap. Historical Development of Water Resources in Australia: Irrigation policy in the
735 Murray-Darling Basin, pp. 28–43, Resources for the Future.

736 Nicholls, N. (2004), The Changing Nature of Australian Droughts, *Climatic Change*,
737 *63*(3), 323–336, doi:10.1023/B:CLIM.0000018515.46344.6d.

738 Nicholls, N., B. Lavery, C. Frederiksen, W. Drosdowsky, and S. Torok (1996), Recent
739 apparent changes in relationships between the El Niño-Southern Oscillation and Aus-

tralian rainfall and temperature, *Geophysical Research Letters*, *23*(23), 3357–3360, doi: 10.1029/96GL03166.

Palmer, J. G., E. R. Cook, C. S. M. Turney, K. Allen, P. Fenwick, B. I. Cook, A. O'Donnell, J. Lough, P. Grierson, and P. Baker (2015), Drought variability in the eastern Australia and New Zealand summer drought atlas (ANZDA, CE 1500–2012) modulated by the Interdecadal Pacific Oscillation, *Environmental Research Letters*, *10*(12), 124,002, doi: http://dx.doi.org/10.1088/1748-9326/10/12/124002.

Palmer, W. C. (1965), Meteorological drought, *Tech. rep.*, US Weather Bureau, Washington, DC.

Pittock, B., D. Abbs, R. Suppiah, and R. Jones (2006), Climatic background to past and future floods in Australia, *Advances in Ecological Research*, *39*, 13–39, doi:10.1016/S0065-2504(06)39002-2.

Pook, M., S. Lisson, J. Risbey, C. C. Ummenhofer, P. McIntosh, and M. Rebbeck (2009), The autumn break for cropping in southeast Australia: trends, synoptic influences and impacts on wheat yield, *International Journal of Climatology*, *29*(13), 2012–2026, doi: 10.1002/joc.1833.

Pook, M. J., P. C. McIntosh, and G. A. Meyers (2006), The Synoptic Decomposition of Cool-Season Rainfall in the Southeastern Australian Cropping Region, *Journal of Applied Meteorology and Climatology*, *45*(8), 1156–1170, doi:10.1175/JAM2394.1.

Post, D. A., B. Timbal, F. H. S. Chiew, H. H. Hendon, H. Nguyen, and R. Moran (2014), Decrease in southeastern Australian water availability linked to ongoing Hadley cell expansion, *Earth's Future*, *2*(4), 231–238, doi:10.1002/2013EF000194.

762 Potter, N. J., F. H. S. Chiew, and A. J. Frost (2010), An assessment of the severity
763 of recent reductions in rainfall and runoff in the Murray–Darling Basin, *Journal of*
764 *Hydrology*, *381*(1–2), 52 – 64, doi:http://dx.doi.org/10.1016/j.jhydrol.2009.11.025.
765 Poulter, B., D. Frank, P. Ciais, R. B. Myneni, N. Andela, J. Bi, G. Broquet, J. G.
766 Canadell, F. Chevallier, Y. Y. Liu, S. W. Running, S. Sitch, and G. R. van der Werf
767 (2014), Contribution of semi-arid ecosystems to interannual variability of the global
768 carbon cycle, *Nature*, *509*(7502), 600–603, doi:10.1038/nature13376.
769 Power, S., F. Tseitkin, S. Torok, B. Lavery, R. Dahni, and B. McAvaney (1998), Australian
770 temperature, Australian rainfall and the Southern Oscillation, 1910-1992: coherent
771 variability and recent changes, *Australian Meteorological Magazine*, *47*(2), 85–101.
772 Power, S., T. Casey, C. Folland, A. Colman, and V. Mehta (1999), Inter-decadal mod-
773 ulation of the impact of ENSO on Australia, *Climate Dynamics*, *15*(5), 319–324, doi:
774 10.1007/s003820050284.
775 Quiggin, J. (2001), Environmental economics and the Murray–Darling river system, *Aus-*
776 *tralian Journal of Agricultural and Resource Economics*, *45*(1), 67–94, doi:10.1111/
777 1467-8489.00134.
778 Risbey, J. S., M. J. Pook, P. C. McIntosh, M. C. Wheeler, and H. H. Hendon (2009),
779 On the Remote Drivers of Rainfall Variability in Australia, *Monthly Weather Review*,
780 *137*(10), 3233–3253, doi:10.1175/2009MWR2861.1.
781 Roderick, M. L., P. Greve, and G. D. Farquhar (2015), On the assessment of aridity
782 with changes in atmospheric CO2, *Water Resources Research*, *51*(7), 5450–5463, doi:
783 10.1002/2015WR017031.

Russell, H. C. (1877), *Climate of New South Wales: descriptive, historical, and tabular*, 252 pp., C. Potter for Government Printer.

Saft, M., A. W. Western, L. Zhang, M. C. Peel, and N. J. Potter (2015), The influence of multiyear drought on the annual rainfall-runoff relationship: An Australian perspective, *Water Resources Research*, *51*(4), 2444–2463, doi:10.1002/2014WR015348.

Scheff, J., and D. M. W. Frierson (2013), Scaling Potential Evapotranspiration with Greenhouse Warming, *Journal of Climate*, *27*, 1539–1558, doi:10.1175/JCLI-D-13-00233.1.

Smerdon, J. E., B. I. Cook, E. R. Cook, and R. Seager (2015), Bridging Past and Future Climate across Paleoclimatic Reconstructions, Observations, and Models: A Hydroclimate Case Study, *Journal of Climate*, *28*(8), 3212–3231, doi:10.1175/JCLI-D-14-00417.1.

Taylor, K. E., R. J. Stouffer, and G. A. Meehl (2012), An Overview Of CMIP5 And The Experiment Design, *Bulletin of the American Meteorological Society*, *93*(4), 485–498, doi:http://dx.doi.org/10.1175/BAMS-D-11-00094.1.

Teague, B., R. McLeod, and P. S (2010), Final report summary of the 2009 Victorian Bushfires Royal Commission, *Tech. rep.*, Government Printer for the State of Victoria.

Theobald, A., H. McGowan, and J. Speirs (2015), Trends in synoptic circulation and precipitation in the Snowy Mountains region, Australia, in the period 1958–2012, *Atmospheric Research*, *in press*, –, doi:http://dx.doi.org/10.1016/j.atmosres.2015.05.007.

Timbal, B., and R. Fawcett (2012), A Historical Perspective on Southeastern Australian Rainfall since 1865 Using the Instrumental Record, *Journal of Climate*, *26*(4), 1112–1129, doi:10.1175/JCLI-D-12-00082.1.

Timbal, B., and R. Fawcett (2013), A historical perspective on southeastern australian rainfall since 1865 using the instrumental record, *Journal of Climate*, *26*(4), 1112–1129, doi:10.1175/JCLI-D-12-00082.1.

Trenberth, K. E. (2011), Changes in precipitation with climate change, *Climate Research*, *47*(1), 123–138, doi:doi:10.3354/cr00953.

Trenberth, K. E., J. T. Fasullo, and T. G. Shepherd (2015), Attribution of climate extreme events, *Nature Climate Change*, *5*(8), 725–730, doi:10.1038/nclimate2657.

Ukkola, A. M., I. C. Prentice, T. F. Keenan, A. I. J. M. van Dijk, N. R. Viney, R. B. Myneni, and J. Bi (2016), Reduced streamflow in water-stressed climates consistent with CO2 effects on vegetation, *Nature Climate Change*, *6*(1), 75–78, doi:doi:10.1038/nclimate2831.

Ummenhofer, C. C., M. H. England, P. C. McIntosh, G. A. Meyers, M. J. Pook, J. S. Risbey, A. S. Gupta, and A. S. Taschetto (2009), What causes southeast Australia's worst droughts?, *Geophysical Research Letters*, *36*(4), n/a–n/a, doi:10.1029/2008GL036801.

Ummenhofer, C. C., A. Sen Gupta, P. R. Briggs, M. H. England, P. C. McIntosh, G. A. Meyers, M. J. Pook, M. R. Raupach, and J. S. Risbey (2011), Indian and Pacific Ocean Influences on Southeast Australian Drought and Soil Moisture, *Journal of Climate*, *24*(5), 1313–1336, doi:10.1175/2010JCLI3475.1.

Ummenhofer, C. C., A. Sen Gupta, M. H. England, A. S. Taschetto, P. R. Briggs, and M. R. Raupach (2015), How did ocean warming affect Australian rainfall extremes during the 2010/2011 La Niña event?, *Geophysical Research Letters*, pp. n/a–n/a, doi:10.1002/2015GL065948.

van den Honert, R. C., and J. McAneney (2011), The 2011 Brisbane Floods: Causes, Impacts and Implications, *Water*, *3*(4), 1149, doi:10.3390/w3041149.

van der Schrier, G., J. Barichivich, K. R. Briffa, and P. D. Jones (2013), A scPDSI-based global data set of dry and wet spells for 1901–2009, *Journal of Geophysical Research: Atmospheres*, doi:10.1002/jgrd.50355.

van Dijk, A. I. J. M., H. E. Beck, R. S. Crosbie, R. A. M. de Jeu, Y. Y. Liu, G. M. Podger, B. Timbal, and N. R. Viney (2013), The Millennium Drought in southeast Australia (2001–2009): Natural and human causes and implications for water resources, ecosystems, economy, and society, *Water Resources Research*, pp. n/a–n/a, doi:10.1002/wrcr.20123.

Vance, T. R., J. L. Roberts, C. T. Plummer, A. S. Kiem, and T. D. van Ommen (2015), Interdecadal Pacific variability and eastern Australian megadroughts over the last millennium, *Geophysical Research Letters*, *42*(1), 129–137, doi:10.1002/2014GL062447.

Verdon-Kidd, D. C., and A. S. Kiem (2009), Nature and causes of protracted droughts in southeast Australia: Comparison between the Federation, WWII, and Big Dry droughts, *Geophysical Research Letters*, *36*(22), n/a–n/a, doi:10.1029/2009GL041067.

Verdon-Kidd, D. C., A. S. Kiem, and R. Moran (2014), Links between the Big Dry in Australia and hemispheric multi-decadal climate variability – implications for water resource management, *Hydrology and Earth System Sciences*, *18*(6), 2235–2256, doi:10.5194/hess-18-2235-2014.

Wei, Y., J. Langford, I. R. Willett, S. Barlow, and C. Lyle (2011), Is irrigated agriculture in the Murray Darling Basin well prepared to deal with reductions in water availability?, *Global Environmental Change*, *21*(3), 906 – 916, doi:http://dx.doi.org/10.1016/j.

851 gloenvcha.2011.04.004, symposium on Social Theory and the Environment in the New
852 World (dis)Order.

853 Williams, A. P., R. Seager, J. T. Abatzoglou, B. I. Cook, J. E. Smerdon, and E. R. Cook
854 (2015), Contribution of anthropogenic warming to the 2012–2014 California drought,
855 *Geophysical Research Letters*, *42*(16), 6819–6828, doi:10.1002/2015GL064924.

856 Young, M. D., and J. C. McColl (2003), Robust Reform: The Case for a New Water
857 Entitlement System for Australia, *Australian Economic Review*, *36*(2), 225–234, doi:
858 10.1111/1467-8462.00282.

**Figure 1.** Loadings for the first three varimax rotated principal components for the eastern Australia portion of the ANZDA. Percentages in the titles indicate the proportion of variance explained by each mode. Dashed boxes indicate our main regions of study over which we generate the regional average PDSI time series from the ANZDA. These correspond to the major centers of loading of the three principal components: Southeastern Australia (PC1; 138°-154°E, 28°-39.5°S), Western Queensland (PC2; 138°-145°E, 18°-28°S), and Coastal Queensland (PC3; 145°-154°E, 18°-28°S).

**Figure 2.** Austral summer (December-January-February; DJF) PDSI from the ANZDA during the Millennium Drought (2003–2009) and 2011 pluvial in eastern Australia. Dashed boxes outline our three primary regions of analysis identified in Figure 1.

**Figure 3.** Correlations (Spearman's rank) between single and cumulative season CRU precipitation and instrumental (top row) and reconstructed (bottom row) regional average summer (December-January-February; DJF) PDSI from the ANZDA. Seasonal subscripts indicate correlations with concurrent (0) or preceding (-1) seasons. Dashed black lines represent the threshold for significance ($p \leq 0.05$, one-sided test for positive correlation).

**Figure 4.** Correlations (Spearman's rank) between the Southeastern Australia reconstructed ANZDA summer (December-January-February; DJF) PDSI and the single and cumulative season historical precipitation from the *Ashcroft et al.* [2014] reconstruction. Seasonal subscripts indicate correlations with concurrent (0) or preceding (-1) seasons. Dashed black lines represent the threshold for significance ($p \leq 0.05$, one-sided test for positive correlation).

**Figure 5.** Seasonal precipitation [*Ashcroft et al.*, 2014] and ANZDA summer (December-January-February; DJF) PDSI anomalies for the three major multi-year historical droughts in Southeastern Australia: the Federation Drought, World War II Drought, and Millennium Drought. PDSI anomalies are based on the standard PDSI scaling, while units for precipitation are standardized anomalies. Subscripts indicate composites of concurrent (0) or antecedent (-1) seasonal anomalies in the multi-year average (relative to the summer).

**Figure 6.** Regional average summer (December-January-February; DJF) PDSI (top) and fractional drought area ($PDSI < 0$) (bottom) from the ANZDA, calculated for our three eastern Australia regions combined: Western Queensland, Coastal Queensland, and Southeastern Australia. Uncertainties in the reconstruction are shown in blue-grey shading, estimated as the $90^{\text{th}}$ percentile prediction intervals from a linear regression between the tree-ring and instrumental PDSI time series over 1902–1929 (the independent reconstruction verification interval). Solid red lines are regional average PDSI and drought area calculated from the instrumental PDSI. Dashed brown lines are the multi-year mean PDSI and drought area associated with the Millennium Drought (2003–2009). Dashed blue lines are the same, but for the 2011 pluvial.

**Figure 7.** Regional average summer (December-January-February; DJF) PDSI for our three eastern Australia regions: Western Queensland, Coastal Queensland, and Southeastern Australia. Uncertainties in the reconstruction are shown in blue-grey shading, estimated as the $90^{\text{th}}$ percentile prediction intervals from a linear regression between the tree-ring and instrumental PDSI time series over 1902–1929 (the independent reconstruction verification interval). Solid red lines are regional average PDSI and drought area calculated from the instrumental PDSI. Dashed brown lines are the multi-year mean PDSI and drought area associated with the Millennium Drought (2003–2009). Dashed blue lines are the same, but for the 2011 pluvial.

**Figure 8.** Reconstructed summer (December-January-February; DJF) PDSI from selected extreme single drought years in the ANZDA. 1519 was the driest year in Coastal Queensland (top 5 driest in Western Queensland and Southeastern Australia), 1565 was the driest in Western Queensland, and 1833 was the driest year in Southeastern Australia (top 5 driest in Coastal Queensland). The drought in 1792 occurred soon after the initial European colonization of the continent. This extreme year ranked among the top 5 driest years in Southeastern Australia and Coastal Queensland.

**Figure 9.** Reconstructed (pre-1975) and instrumental (post-1975) summer (December-January-February; DJF) PDSI for the Millennium Drought (2003–2009) and the driest 7-year running mean PDSI periods in each region: Southeastern Australia (1508–1514), Coastal Queensland (1514–1520), and Western Queensland (1560–1566). Note the reduced range on the colorbar compared to Figure 8.

**Figure 10.** Reconstructed (pre-1975) and instrumental (post-1975) summer (December-January-February; DJF) PDSI for extreme wet years in the ANZDA: 1572 (top 5 wettest in Southeastern Australia and Western Queensland), 1573 (top 10 in all three regions), 1974 (top 5 in Western Queensland and Southeastern Australia), and 1976 (top 10 in all three regions).

**Figure 11.** Left column: empirical 20th century (1902–1975) cumulative distribution functions (CDFs) from the ANZDA (tree-ring reconstructed and instrumental) and CMIP5 ensemble. For the ANZDA, n= 74 (one realization of the historical record in the observations); for CMIP5 n= 3400 (34 different ensemble-member simulations from 1902–1974). Using a 2-sided Kolmogorov-Smirnov test, we conclude there is no significant difference ($p \geq 0.05$) in the underlying distributions between either ANZDA series and the CMIP5 ensemble for this interval. Center column: number of major drought (PDSI$\leq -1$) and pluvial (PDSI$\geq +1$) years in the ANZDA (tree-ring reconstructed and instrumental; green and red dots, respectively) and CMIP5 ensemble (boxplot; 34 different ensemble-member simulations) for the same time interval. Right column: distributions of droughts lengths (years) from the ANZDA (1500–2012) and CMIP5 ensemble (1901–2012), determined using the 2S2E criteria.

**Figure 12.** Late 21st century (2050–2099, RCP 8.5 scenario) mean summer (December-January-February; DJF) PDSI for our three regions, calculated from 34 simulations of 15 models in the CMIP5 archive. Each model is represented by a color, and individual bars within a color represent different ensemble member simulations of the same model (a consequence of different initial conditions). These PDSI projections incorporate model trends in both precipitation and potential evapotranspiration over the 21st century.

**Figure 13.** Time series of the ensemble summer (December-January-February; DJF) PDSI (historical+RCP 8.5, 1901–2099) for our three regions, from the same models in Figure 12. The solid blue line is the ensemble average PDSI only incorporating model trends in precipitation, with the associated ensemble spread (cross model interquartile range) shown by the blue dashed lines. The solid red line is the ensemble average PDSI calculated using trends in both precipitation and potential evapotranspiration, with the associated ensemble spread (cross model interquartile range) in the gray shading.

**Figure 14.** Cumulative kernel density functions for summer (December-January-February; DJF) PDSI, calculated from the ANZDA (1500–2012) and the CMIP5 multi-model ensemble (1901–2000, 2020–2049, 2050–2099). Vertical lines indicate PDSI values in the ANZDA for 2011 (blue), and the record driest year for each region (brown).

**Figure 15.** Cumulative kernel density functions for summer (December-January-February; DJF) PDSI calculated on 7-year moving window average PDSI. Vertical lines indicate PDSI values for 2003–2009 (Millennium Drought) and the driest 7-year moving average PDSI in each region.

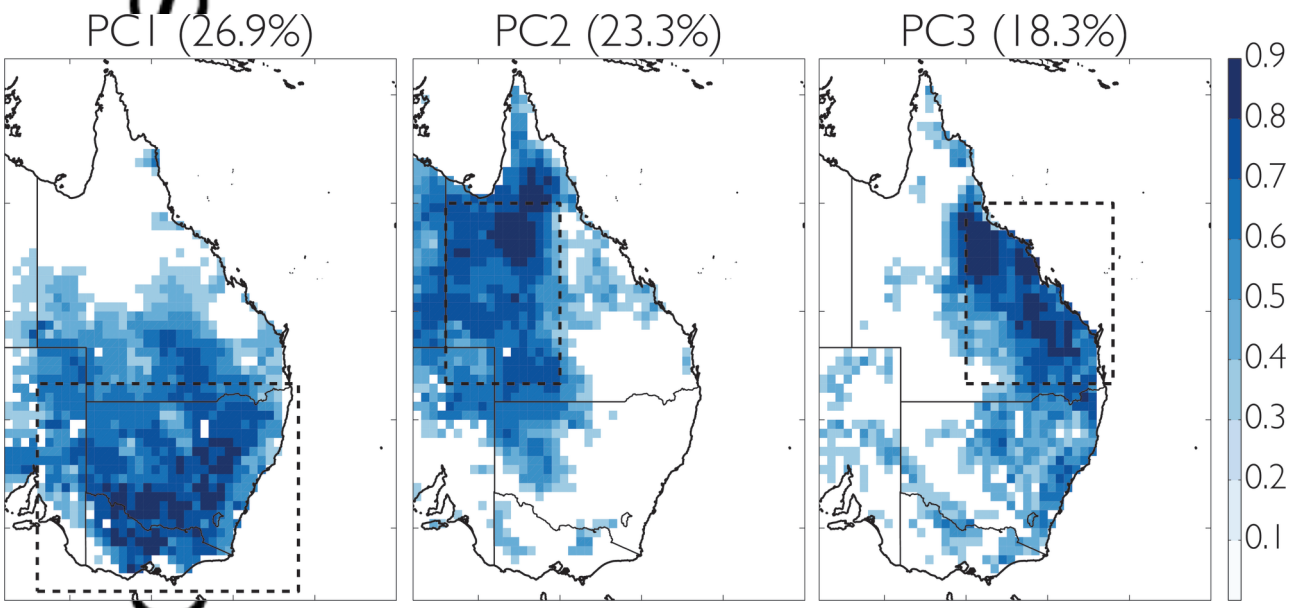


2016jd024892-f01-z-.eps

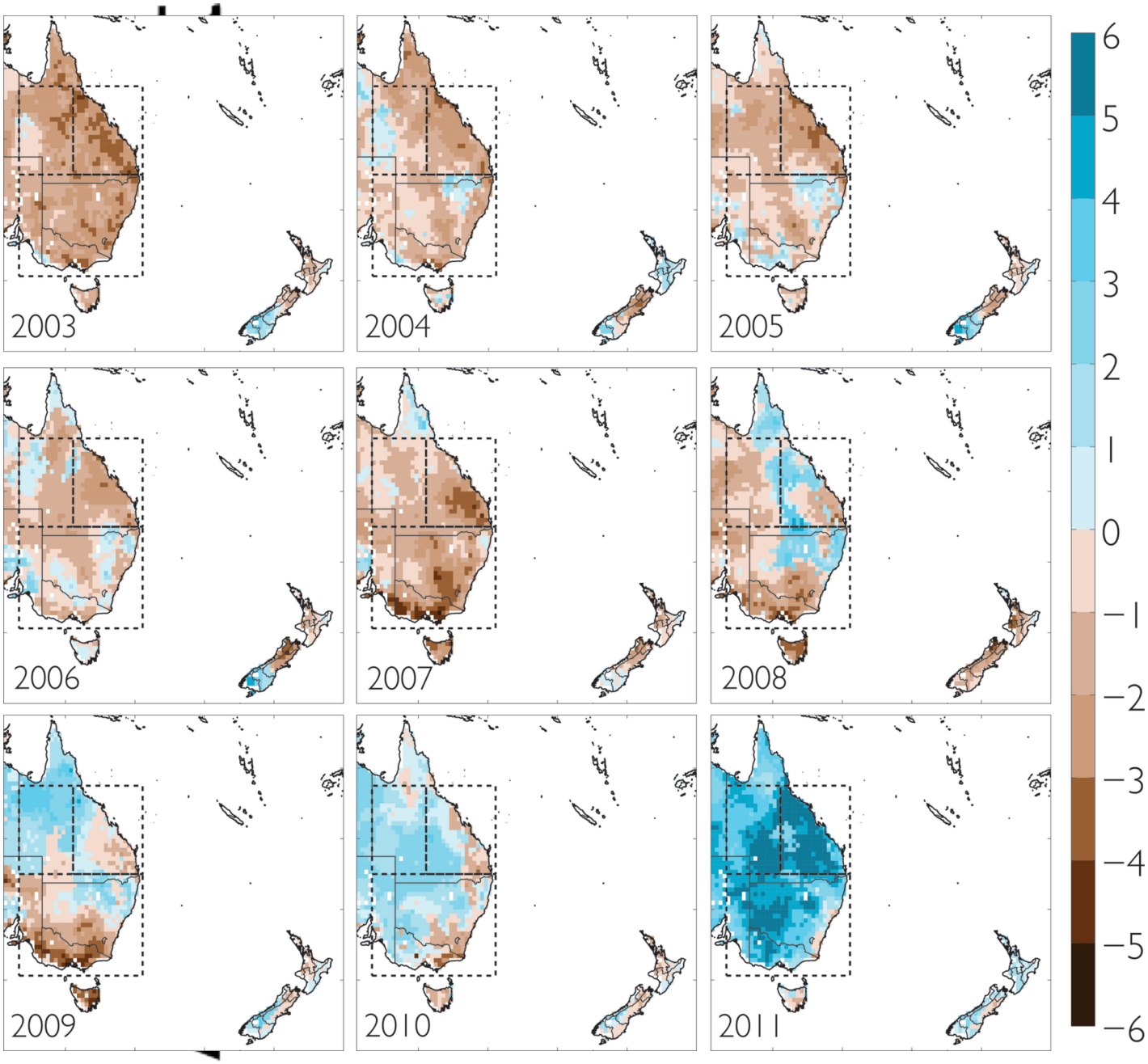


2016jd024892-f02-z-.eps

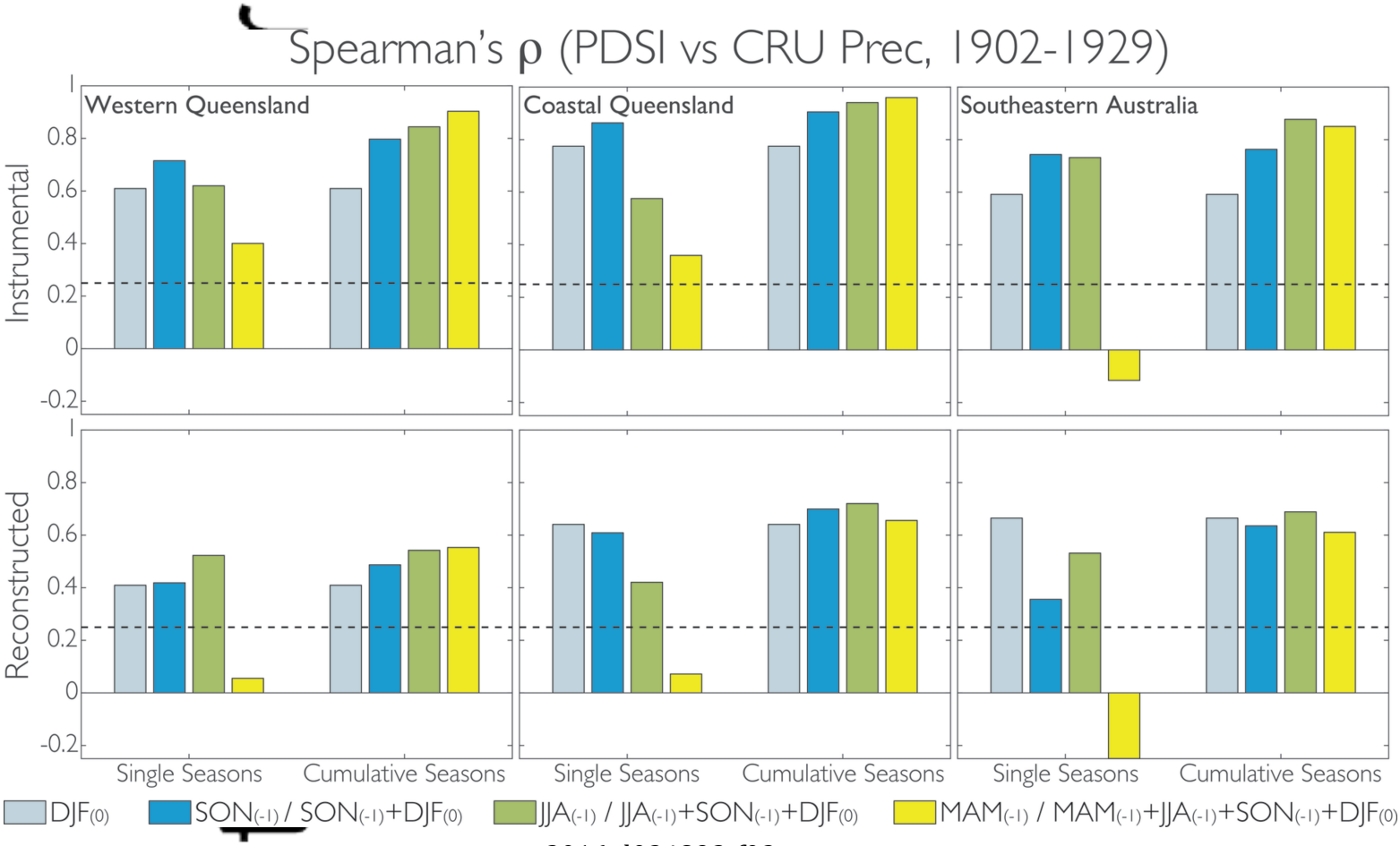


2016jd024892-f03-z-.eps

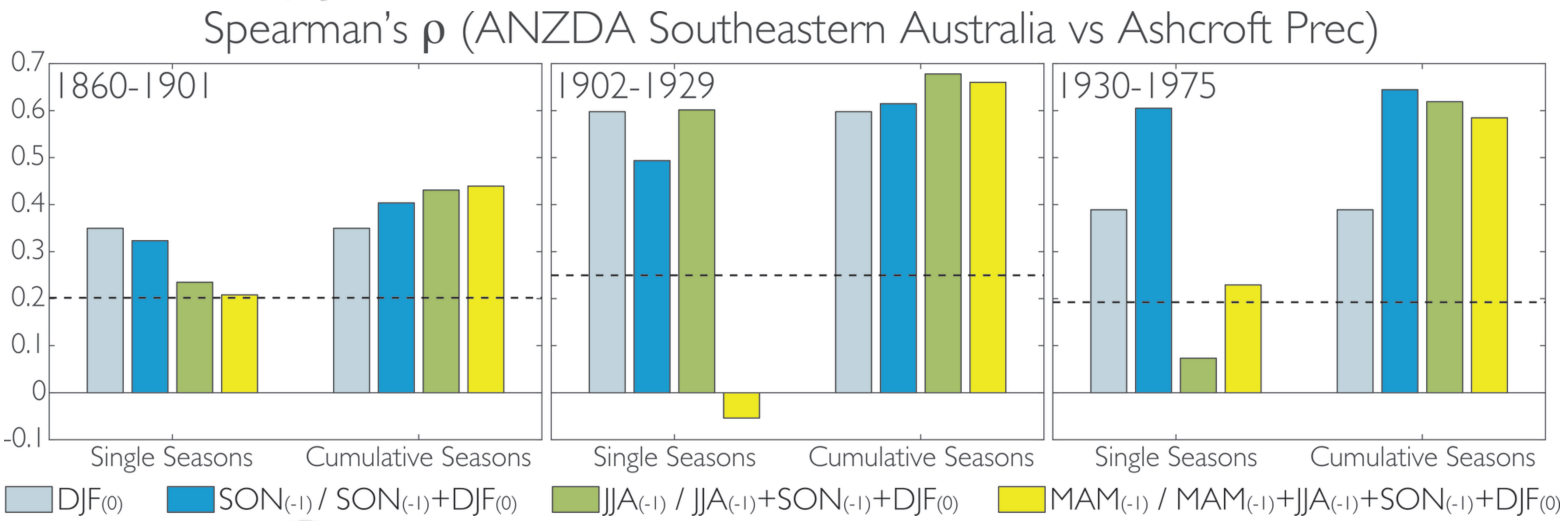


2016jd024892-f04-z-.eps

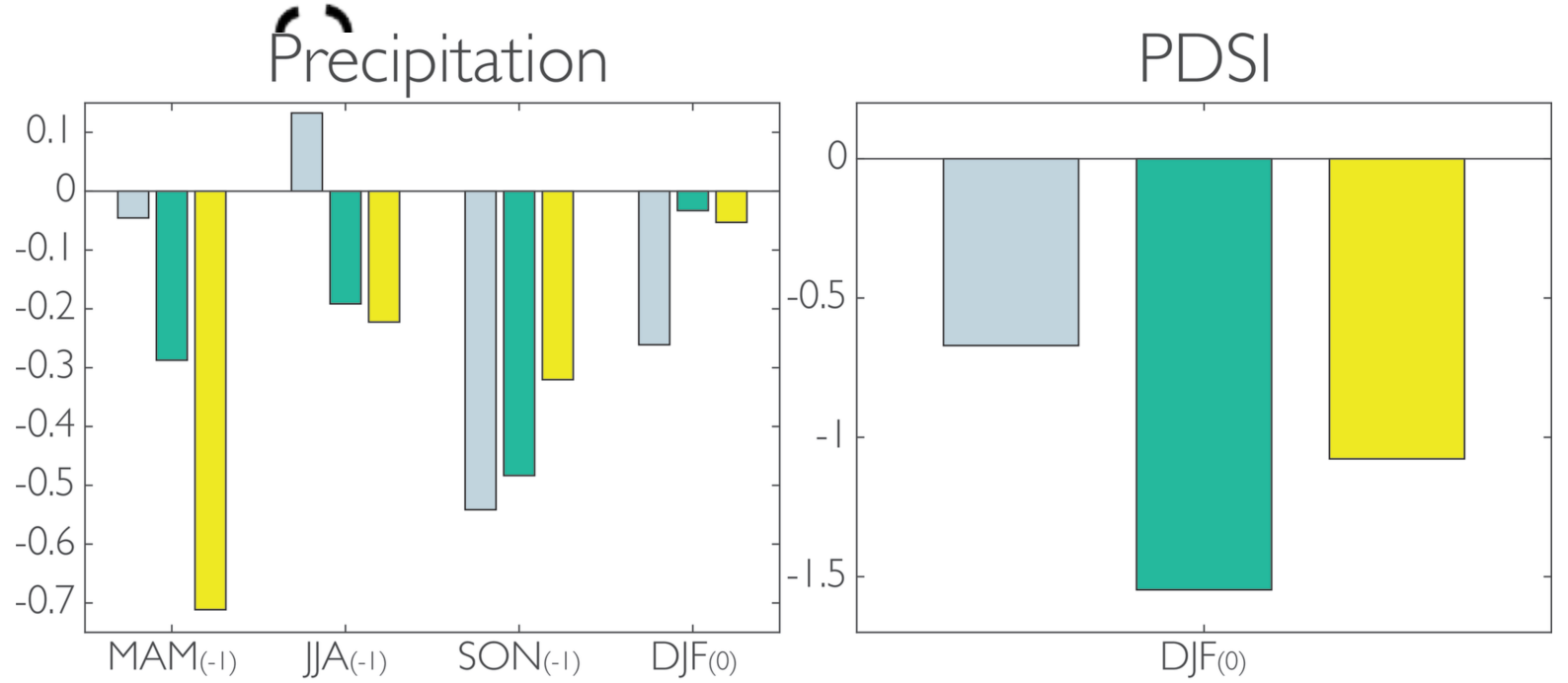


2016jd024892-f05-z-.eps

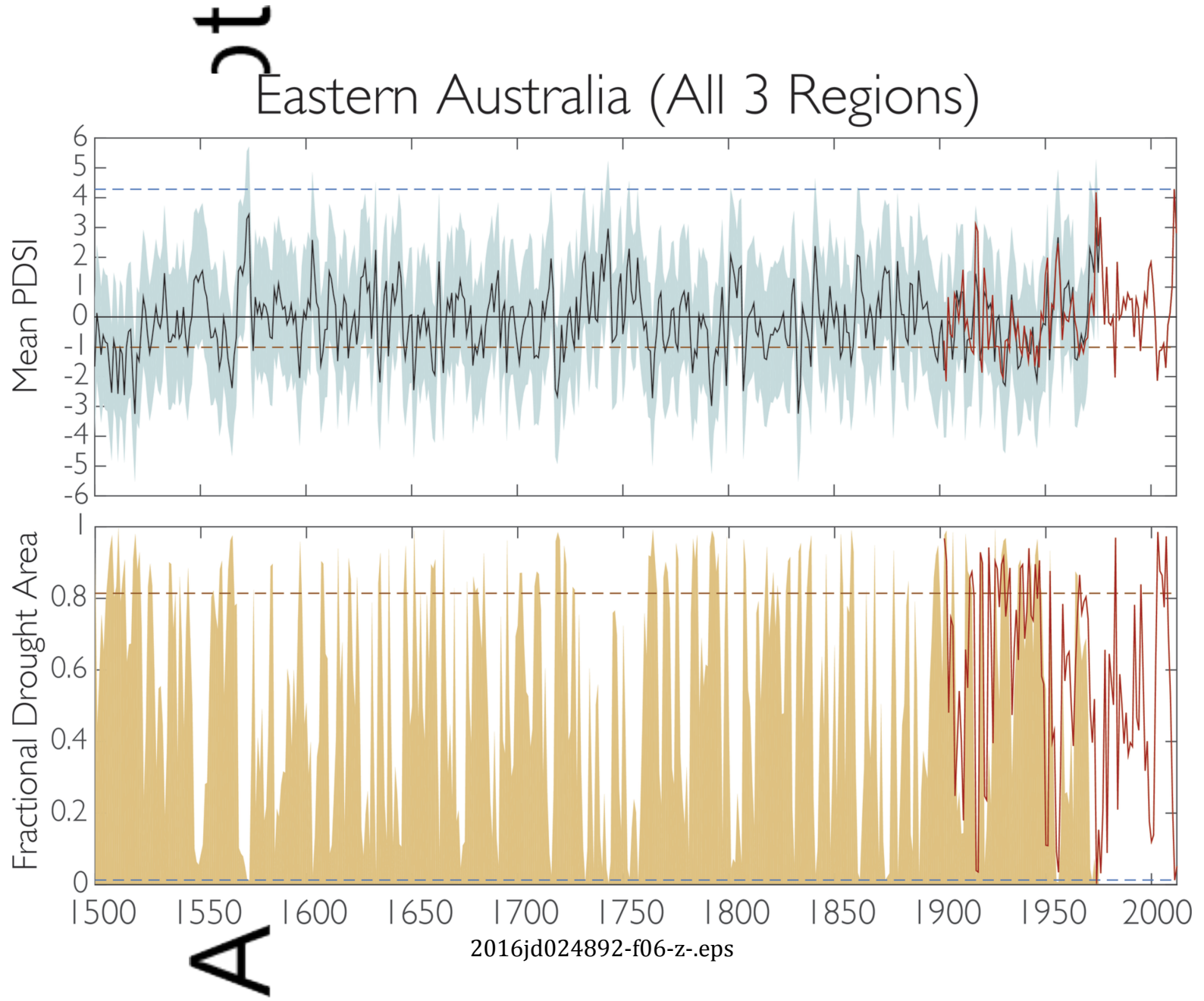


2016jd024892-f06-z-.eps

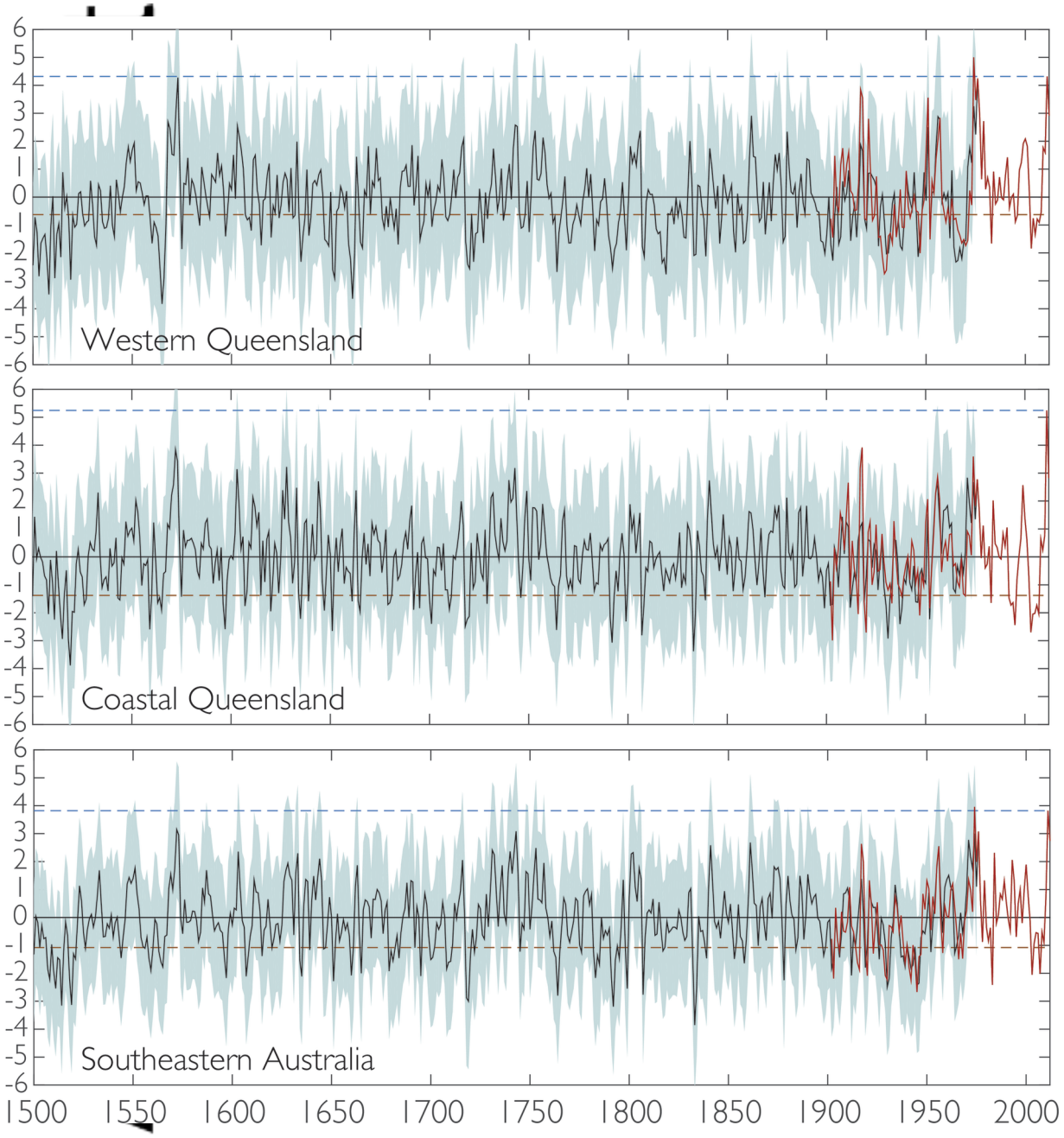


2016jd024892-f07-z-.eps

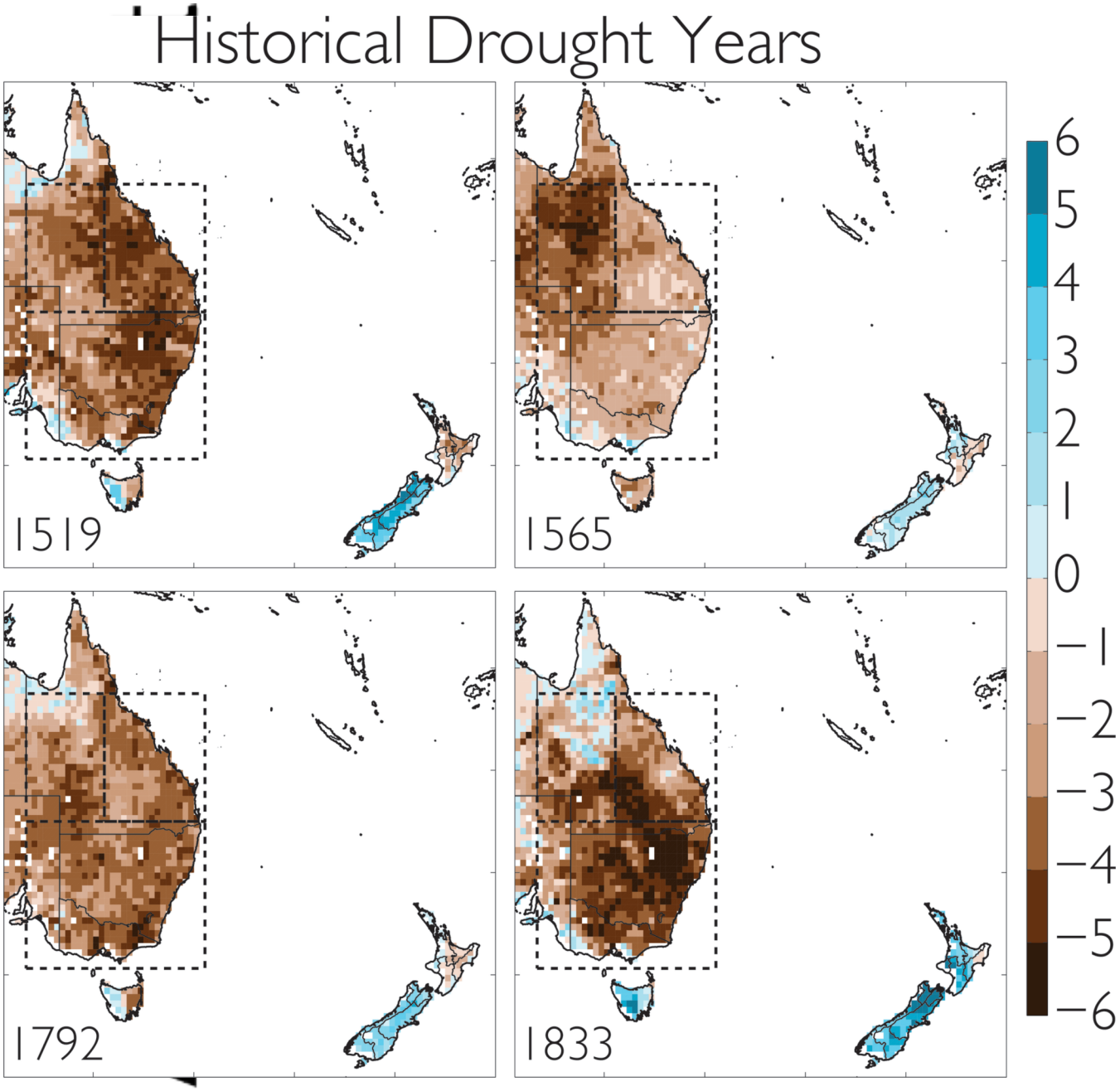


2016jd024892-f08-z-.eps

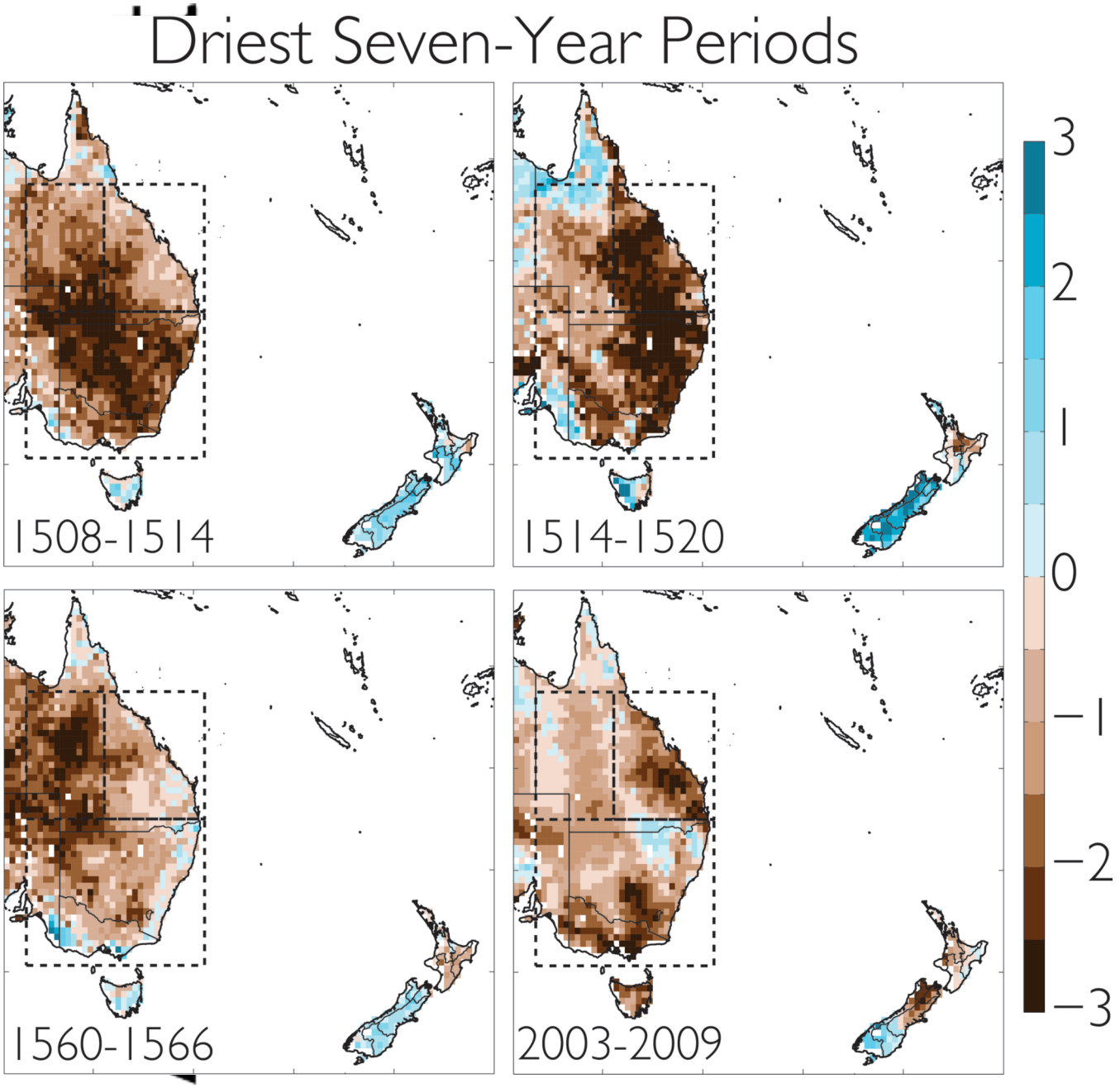


2016jd024892-f09-z-.eps

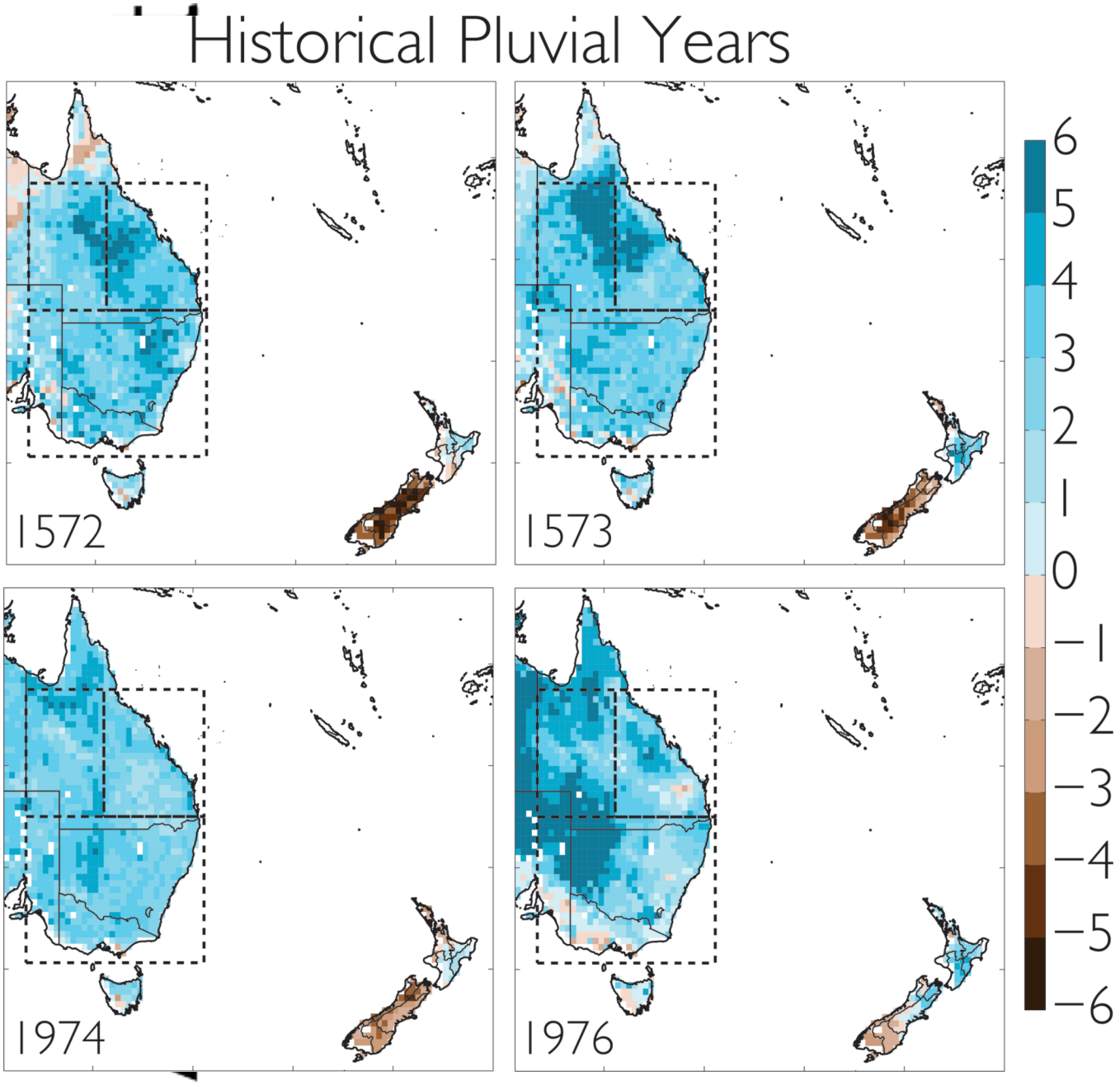


2016jd024892-f10-z-.eps

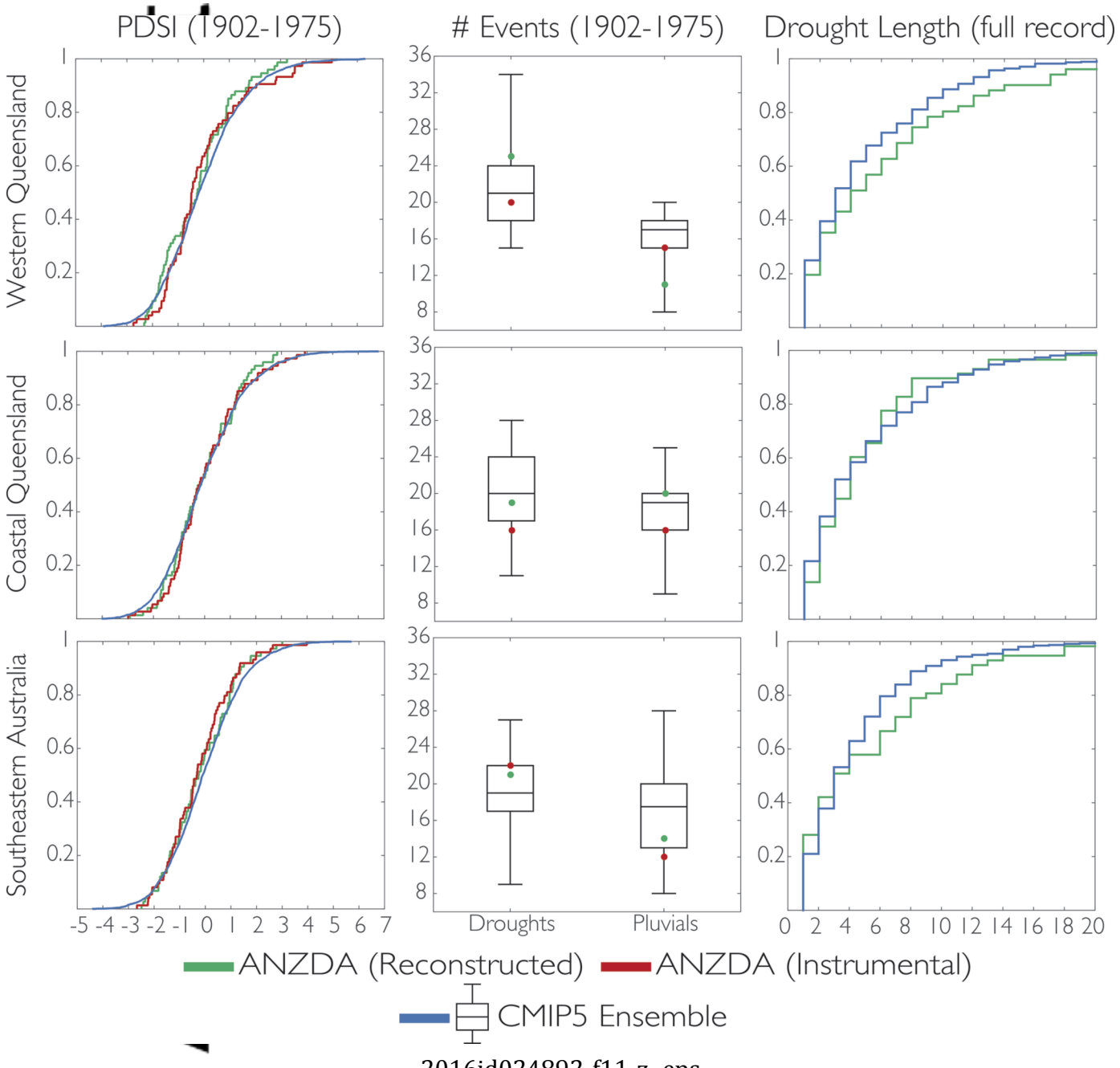


2016jd024892-f11-z-.eps

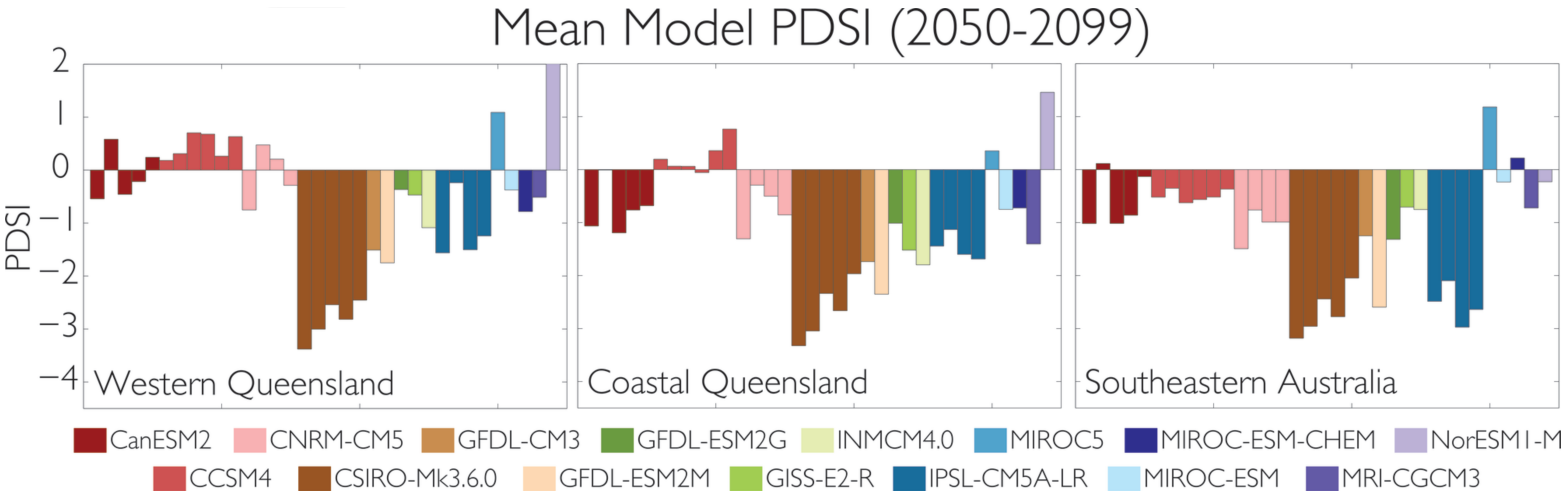


2016jd024892-f12-z-.eps

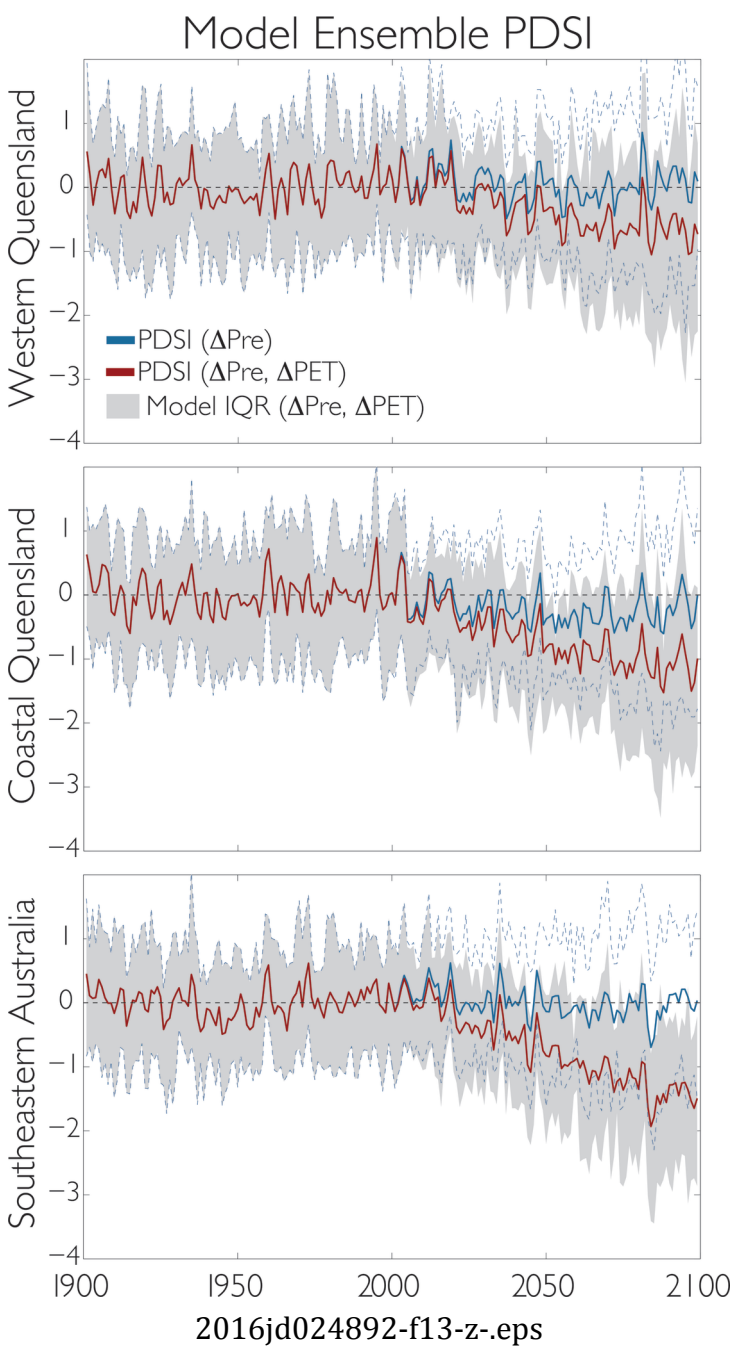


2016jd024892-f13-z-.eps

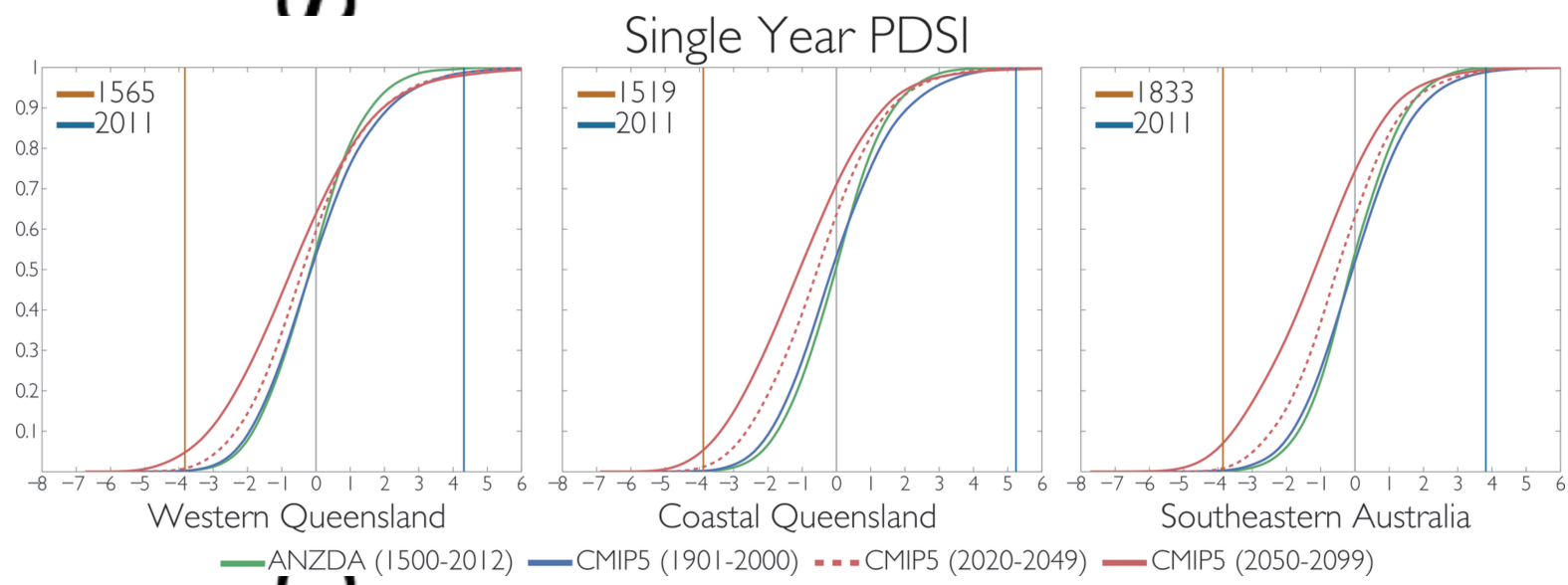


2016jd024892-f14-z-.eps

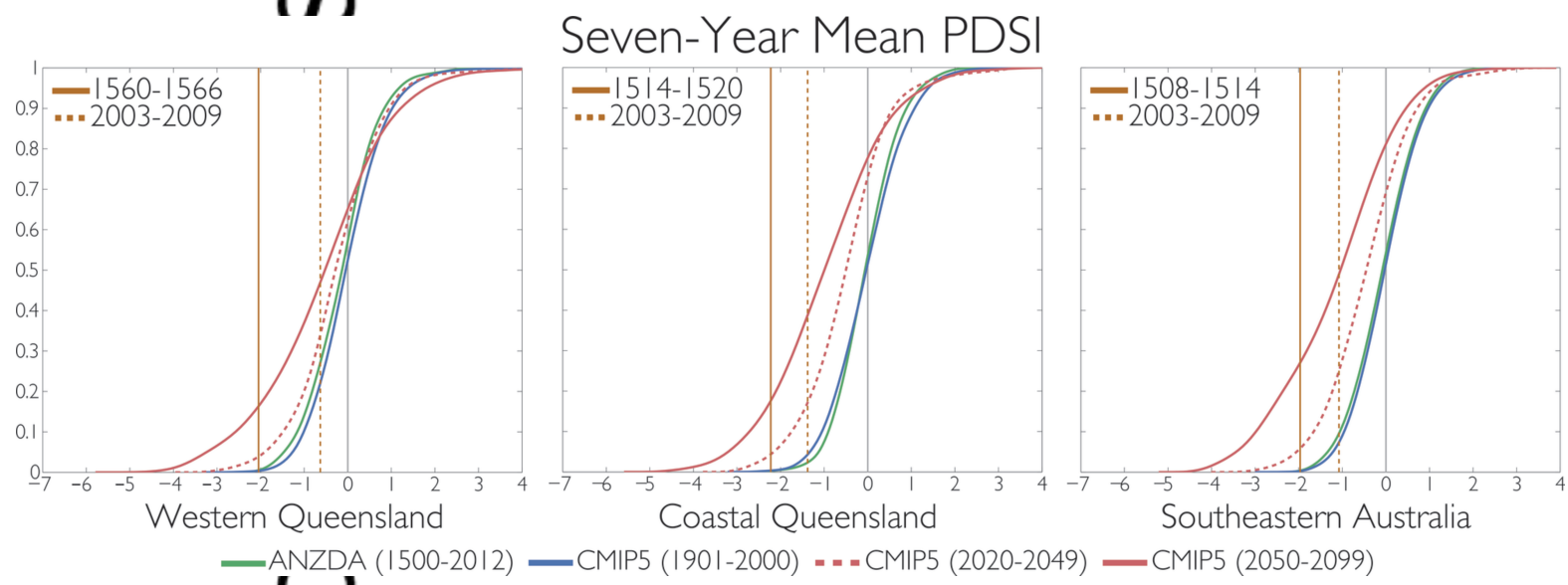


2016jd024892-f15-z-.eps